

66280

GALACTIC BACKGROUND MAPS AT 3.93 AND 6.55 MHz

(NASA-TN-X-66280) GALACTIC BACKGROUND
MAPS AT 3.93 AND 6.55 MHz M.S. Thesis
- Maryland Univ. (NASA) 147 p HC \$9.50
148

N73-27728

CSCL 03B

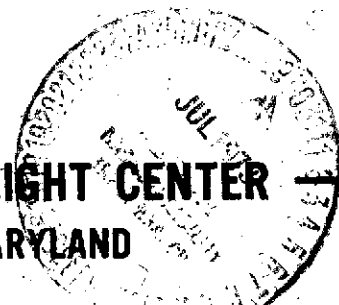
Unclass
G3/30 09207

JAMES C. NOVACO

JUNE 1973

GSFC

**GODDARD SPACE FLIGHT CENTER
GREENBELT, MARYLAND**



GALACTIC BACKGROUND MAPS AT 3.93 AND 6.55 MHz

by
James Charles Novaco

Dissertation submitted to the Faculty of the Graduate School
of the University of Maryland in partial fulfillment
of the requirements for the degree of
Master of Science
1973

I

ABSTRACT

Title of Thesis: Galactic Background Maps at 3.93 and 6.55 MHz.

James Charles Novaco

Thesis directed by: Professor Frank J. Kerr

The Radio Astronomy Explorer Satellite (RAE-1), its hardware and its data processing are discussed. The data from the prime mapping antenna are discussed with emphasis on the problems involved in reducing the data. Particular attention is drawn to two problems - receiver instability and ground breakthrough - and their influence on the data.

Galactic background maps of the nonthermal radiation at 3.93 and 6.55 MHz are produced. At 3.93 MHz, the main lobe of the antenna beam is approximately $23^{\circ} \times 52^{\circ}$ and about $14^{\circ} \times 34^{\circ}$ at 6.55 MHz. It is demonstrated that the positional uncertainty of the maps is about 20° . The maps at 3.93 and 6.55 MHz are compared to two ground based maps made at higher frequencies that are smoothed to the larger RAE antenna patterns.

In the background maps at 3.93 and 6.55 MHz, neither the Gould Belt nor the Galactic Equator are very obvious.

At 3.93 MHz there are three prominent features. The Orion-1 complex shows up as a large region in absorption. The region extends further north of the galactic plane than does the HII complex. At lower declinations the feature is possibly blended with a feature attributed to the Gum Nebula. There is a region of emission centered roughly on the II Sco Association. Finally, there is a gradient running from about 22^h to 14^h , north of declinations above $+15^\circ$. There is some weak evidence that the North Galactic Spur and the Cetus Arc are visible in the maps.

The same three features are prominent in the 6.55 MHz map. However, the gradient is restricted to the region from about 22^h to 17^h , north of $+15^\circ$ declination. The emission region, that at 3.93 MHz is centered roughly on the II Sco Association, is at 6.55 MHz enlarged to include the base of the North Galactic Spur and is probably a blend of the two features. The Orion-1 complex is still present in absorption at 6.55 MHz, but is now greatly elongated perpendicular to the galactic plane.

PREFACE

Ground based low frequency radio astronomy has shown the need for doing extensive research at frequencies below the typical ionospheric cutoff. Such research must be done with instruments placed above the ionosphere. Such long term projects such as galactic background long term spectral and solar studies dictate the use of a satellite.

The Radio Astronomy Explorer Satellite was launched on July 4, 1968 to provide data to answer at least some of the questions brought about by ground based low frequency radio astronomy. This thesis is an analysis of some of the data from the satellite to produce a map of the galactic background.

In the introduction (Chapter I), I have tried to show the reasons why such low frequency observations are necessary and the problems involved in making galactic observations. I have tried to place the Radio Astronomy Explorer Satellite and this thesis in a historical perspective.

Chapter II is a discussion of the satellite. It discusses the technique used to stabilize and point the satellite.

The Vee antennas, the Ryle-Vonberg receivers, and the calibration procedures are discussed. The chapter concludes with a brief discussion of the system reliability.

Chapter III discusses the computer programs that are used to process and reduce the telemetered data. It is broken down into three sections: the tracking station, the Information Processing Division's role in processing the telemetry data, and the Radio Astronomy Branch's programs to reduce the data.

The fourth chapter is an analysis of the Vee antenna data. Particular attention is drawn to the problems associated with these data and the methods used to correct the data, to eliminate or reduce the influence of these problems. Two problems - receiver instability and ground breakthrough - are discussed in detail.

Chapter V presents a map of the sky between the declination limits of $\pm 60^\circ$ for two frequencies - 3.93 and 6.55 MHz. They are compared with ground based maps at higher frequencies that are smoothed to the larger RAE antenna pattern. Also included is a map of the objects that one might expect to see at these low frequencies. It is included to allow

the reader to make his own comparison.

Finally in the Appendix, the plans for the second Radio Astronomy Explorer Satellite are briefly discussed.

At this time, I would like to take this opportunity to express my gratitude to the many people who have helped me. To J.K. Alexander, F.J. Kerr, W.C. Erickson, and T.A. Matthews, who were my advisory committee, I am particularly grateful for their assistance and guidance. J.K. Alexander deserves particular mention for suggesting this project and for the close co-operation that he provided.

I would like to thank R.G. Stone and N.F. Ness for offering me the opportunity to join the staff of Goddard's Radio Astronomy Branch. This project was started while I was a member of the Information Processing Division of Goddard. I would like to thank F.A. Keipert, A.C. Rosenberg, and D.A. Parker for their generosity in allowing me to spend part of my time on a project not related to the functions of their division.

Finally I wish to express my appreciation to all those who I have not yet mentioned, but who contributed to this thesis in ways too numerous to enumerate here.

TABLE OF CONTENTS

CHAPTER	PAGE
PREFACE.	ii
I. INTRODUCTION	1
II. THE OBSERVATORY	6
A. The Satellite As An Observing Platform . . .	9
B. The Vee Antennas	14
C. Receivers on the Upper Vee	19
D. Calibration Procedures	27
E. The Telemetry System	34
F. System Reliability	37
III. GROUND DATA PROCESSING	41
A. Tracking Station	41
B. Information Processing Division	42
C. Radio Astronomy Branch Processing	45
IV. THE UPPER VEE DATA	56
A. Ground Breakthrough	58
B. Glitches	59
C. Receiver Stability	63
D. Correction for Receiver Instability	74
V. THE MAPS FOR 3.93 AND 6.55 MHz	90
VI. SUMMARY	125
THE APPENDIX. THE RAE-B SATELLITE	129
REFERENCES CITED	134

LIST OF TABLES

TABLE		PAGE
1	Errors in absolute calibration of radiometers	35
2	A list of stromgren spheres calculated by Prentice and ter Haar	110
3	A list of HII Regions Larger than 5 degrees	111
4	References for Figure 23	112

LIST OF FIGURES

FIGURE		PAGE
1	The External Configuration of RAE-1 Showing the Antenna and Libration Booms	8
2	A Sample of Raw Data for 3.93 MHz from February 2-3, 1970	11
3	Antenna Pattern of the Vee Antenna for 1.31, 3.93 and 6.55 MHz	18
4	A Block Diagram of the Ryle-Vonberg Receivers	25
5	Typical Calibration Curves for the Ryle- Vonberg Receivers	29
6	Examples of the Variation of the Output of the Ryle-Vonberg Receivers with Environmental Temperature	32
7	A Schematic Time Line of the History of RAE-1	39
8	A Sample of the Histogram Program's Output	48
9	A Sample of the Boxave Program's Output	53
10	A Sample of Raw Data for 3.93 MHz	61
11	A Plot of the Long Term Environmental Temperature Variation of the RV Receivers	65
12	The Long Term Response to the Galactic Background of RV2	68

FIGURE		PAGE
13	A Schematic Diagram Indicating a Possible Change in the Shape of the Calibration Curves	73
14	A Plot of the Equivalent Antenna Temperature As A Function of Right Ascension	78
15	The Penticton 10 MHz Map Convolved with the Vee Antenna Pattern at 3.93 MHz . .	83
16	The Parkes 30 MHz Map Convolved with the Vee Antenna Pattern at 3.93 MHz	84
17	The Penticton 10 MHz Map Convolved with the Vee Antenna Pattern at 6.55 MHz . .	86
18	The Parkes 30 MHz Map Convolved with the Vee Antenna Pattern at 6.55 MHz	88
19	A Map of the Galactic Background at 3.93 MHz	93
20	A Map of the Galactic Background at 6.55 MHz	95
21	A Comparison of the Equivalent Antenna Temperature for RV1 and RV2	99
22	A Plot of the Normalized Equivalent Antenna Temperature	103
23	A Map of the Objects One Might See at Low Frequencies	108
24	The First Preliminary Map of the Galactic Background at 3.93 MHz Using All of the Available Data	121

FIGURE

PAGE

25	The First Preliminary Map of the Galactic Background at 6.55 MHz Using All of the Available Data	123
----	--	-----

I. INTRODUCTION

At low frequencies, that is below about 30 MHz, the ionosphere becomes increasingly opaque. While the actual cutoff is a function of time of day, season, solar cycle and latitude, below 10 MHz the ionosphere remains practically opaque except for a few places on earth. In order to do extensive observations, particularly near or below 1 MHz, one is forced to go into space to get above the ionosphere.

Also, at these low frequencies, many of the normally measurable parameters (position, structure, polarization, spectra, etc.) of discrete sources cannot be measured with today's technology. For instance, to do accurate position, source size, and structure measurements, one would need very large antennas (of the order of 100 km for a resolution of one minute of arc at 10 MHz). If the real estate problems don't overcome you, the engineering and ionospheric problems will. Even in space, if an antenna of this size were possible, coronal scattering would greatly reduce its usefulness.

Why then bother with doing observations at these low frequencies, particularly if there seems to be no hope of

attaining the angular resolution enjoyed by astronomers at higher frequencies? Below about 1400 MHz, the nonthermal component of the Galaxy's diffuse emission and discrete sources begin to dominate the spectrum. One can now map the Galaxy in its nonthermal component to try to get information on its general magnetic field and synchrotron emissivity. One of the biggest problems, as with most radio continuum studies, is to separate the foreground and background objects.

Below 50 MHz, galactic HII regions become optically thick and begin to dominate the observed structure. For large scale mapping, this can confuse the issue, since one is never sure whether a drop in emission is real or caused by an absorbing HII region being in the beam. This has the advantage that, in the direction of nearby HII regions that fill the beam, where the path length over which the radiation is being integrated is reasonably well known, one can get a good handle on quantities like the synchrotron volume emissivity.

At these frequencies, several surveys have already been made, in particular, there is the Penticton 10 MHz map (Purton, 1972) the Parkes 30 MHz map (Mathewson et al, 1965), the Cambridge 13 MHz (Andrew, 1969), the Tasmanian map at

4.7 MHz (Ellis and Hamilton, 1966), and Reber's map at 2.1 MHz (Reber, 1968). They show the galactic equator and such nearby structures as the North Galactic Spur clearly delineated. Large HII complexes such as the Cygnus-X, Orion and Gum Nebula complexes stand out prominently as regions of absorption.

At very low frequencies, that is, well below 10 MHz, even the general interstellar medium begins to become optically thick in a relatively short distance. There is then no major problem separating distant objects from nearby emitting regions. Since at these low frequencies one is seeing emission exclusively from nearby regions, one can map the nearby structure. But to do this mapping requires a large antenna or array situated outside the earth's ionosphere. With today's technology, it does not seem possible to construct and operate either a large antenna or array that would be capable of working at an angular resolution of a few degrees of arc. But even a map of a large fraction of the sky with a more modest angular resolution of an order of magnitude better than a dipole would be a significant step toward obtaining a better understanding of the Galaxy's nearby structure.

It is also at these frequencies that the nonthermal spectrum of the galactic radiation reaches its peak and turns over. Yet, as late as 1964, the spectrum at these frequencies was not well established (Mills 1964). This is mainly because the ionosphere plays such a large perturbing role that the observations should be done above the ionosphere. It has been only recently that extended observations of the galactic low frequency spectrum have been reported in the literature (e.g. Brown 1973a; Alexander et al., 1970; and Clark et al., 1970).

The spectral region below the turnover is dominated by free-free absorption from the interstellar medium's ionized components. Observations of the low frequency spectra for different directions can be the basis for the construction of a model of the interstellar medium's ionized components (Novaco and Vandenberg 1972), and can possibly be used to distinguish between the two more popular models of the interstellar medium (Field et al., 1969; and Hjellming et al., 1969).

By the mid-1960's several groups had conducted some experiments using receivers on board satellites and sounding

rockets (Hartz, 1964; Walsh et al., 1964, etc.). It was during this pioneering era that the Radio Astronomy Explorer Satellite (RAE) was designed. Its goal was to provide reliable and accurate radio astronomy measurements of the low frequency galactic background spectra and to map the background with at least an order of magnitude better resolution than is provided by a dipole antenna.

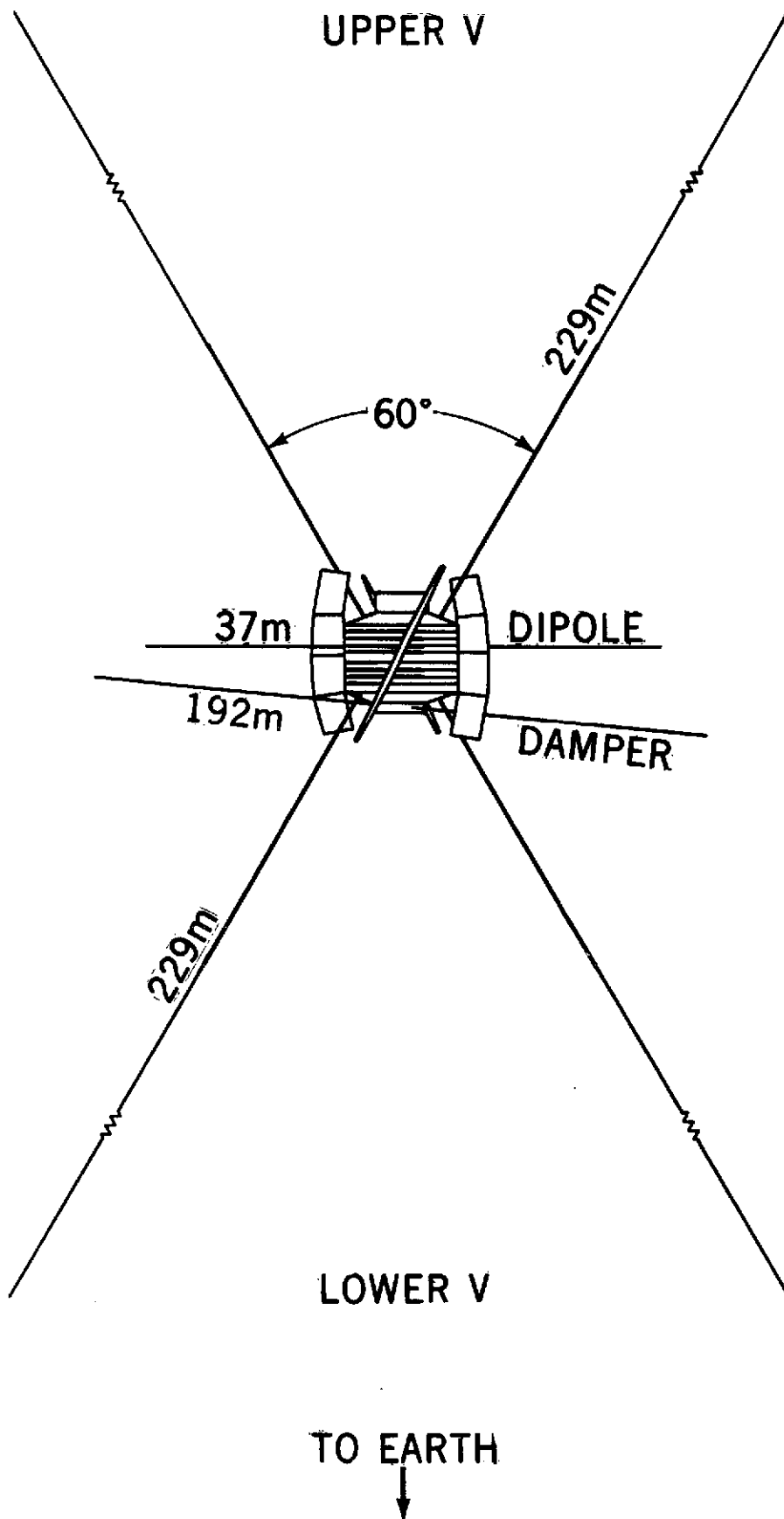
This thesis is an analysis of the data from the RAE Vee antenna for the calendar year 1970 in order to produce a map of the sky scanned by RAE in that year. It includes a discussion of the satellite, the Ryle-Vonberg receivers, the Vee antenna, the calibration procedures, and a description of the computer programs necessary to reduce the data. In the fourth chapter the Vee antenna data are discussed fully with an emphasis on the problems encountered with the data and the attempts to overcome them. The fifth chapter presents a map of the sky for two frequencies - 3.93 and 6.55 MHz that is the result of this analysis of the Vee antenna data. The maps have some similarities with maps at higher frequencies however they are not just an extrapolation from higher frequencies with no new features.

II. THE OBSERVATORY

RAE-1 is the first satellite designed exclusively for low frequency radio astronomy. Since its launch on July 4, 1968, it has sent back data on solar, magnetospheric and galactic low frequency radio phenomena. The satellite consists of two 229 meter travelling wave Vee antennas aligned back-to-back, and a 37 meter dipole bisecting the axis of the Vees. The configuration is shown in Figure 1. (Taken from Weber, Alexander and Stone, 1971, hereinafter called WAS.) The additional boom shown is a 192 meter libration damper used to damp out attitude oscillations about the axes of the satellite.

The upper Vee antenna is equipped with two Ryle-Vonberg radiometers operating at 9 frequencies between 0.45 and 9.18 MHz. The Ryle-Vonberg receiver was chosen because its relative insensitivity to gain and bandwidth changes provides the stability necessary for sky mapping over many months of unattended operation. This receiver measures the antenna signal level by constantly comparing it with an internal voltage-controlled and calibrated noise source that is

Figure 1. - The external configuration of RAE-1 showing the antenna and libration booms. Taken from Weber, Alexander and Stone, 1971, Radio Science, 6,1085.



adjusted by a servo loop until its output is equal in magnitude to the antenna signal.

Each frequency is sampled every 72 seconds with a sample consisting of seven measurements. Once every 10 minutes a calibration is done in which the impedance of the upper Vee is measured.

Figure 2 shows a sample of data for 3.93 for one orbit. The two periods of intense radio emission between 23:20 and 01:00 GMT is stronger on the lower Vee than the upper Vee indicating that it originated below the satellite. This has been termed ground breakthrough since it is terrestrial noise reaching the satellite where the ionosphere has become transparent.

A. The Satellite As An Observing Platform

RAE-1 is stabilized by gravity-gradient forces produced by the stronger gravitational attraction for the lower Vee than for the upper Vee. Consequently, the lower Vee always points toward the earth and the upper Vee toward the local zenith. It is kept pointed to the zenith to within $\pm 3^\circ$ (WAS).

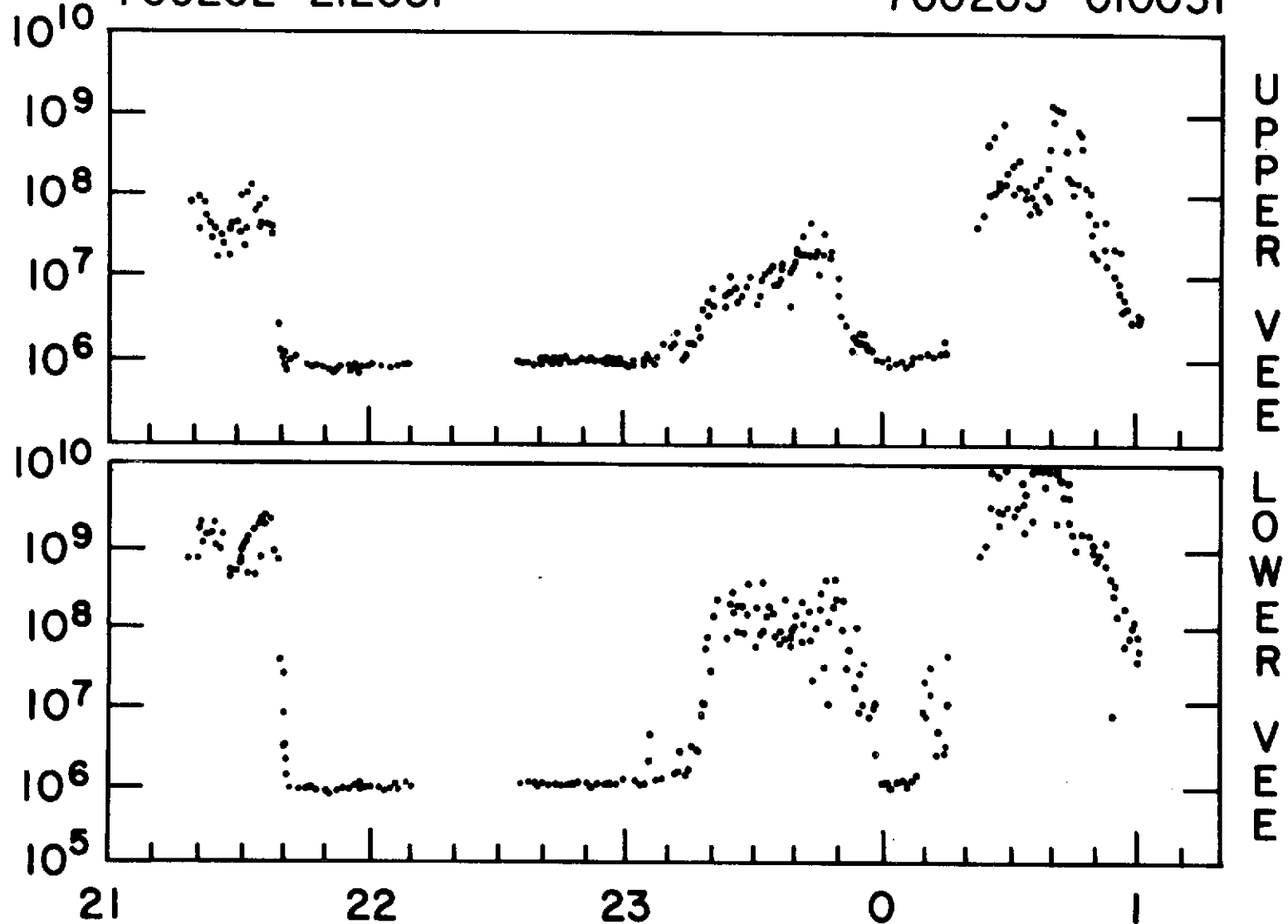
Figure 2. - A sample of raw data for 3.93 MHz from February 2-3, 1970 showing ground breakthrough at 23:20 and 01:00 Greenwich Mean Time.

FREQUENCY 3.93 MHz

START TIME
700202 212031

STOP TIME
700203 010051

CALIBRATED ANTENNA TEMPERATURE (°K)



GREENWICH MEAN TIME
IN HOURS

Coverage of the sky is accomplished by means of the combination of orbital motion and precession of the orbital plane. An orbit with a high inclination and a high precession rate was chosen to provide for the largest amount of sky coverage in the shortest amount of time. The satellite was placed in a retrograde circular orbit 6000 km above the earth's surface with an inclination of 59° . This orbit has a precession rate of $0.52^{\circ}/\text{day}$, requiring nearly two years to completely map the sky between the declination limits of $\pm 60^{\circ}$.

Because of varying thermal conditions, a slightly eccentric orbit, and perturbation in the gravitational field, there are small oscillations of the satellite about its equilibrium positions.

Oscillations about the spin axis of the Vees are damped by the nutation damper within the central body of the spacecraft. The spin axis is normal to the plane of the orbit. Damping of oscillations about the other two axes is provided by the libration damper. This consists of a 192 meter boom rigidly attached to a magnetic hysteresis damper, which dissipates the energy of the oscillations. Details of the construction

and operation of the dampers are given by Mattingly et al. (1970).

Since the final deployment of the booms, the attitude of the central spacecraft body has been well behaved. A thorough study of the attitude data was made shortly after the final deployment (Blanchard, 1969). This indicated that the motions have been generally less than $\pm 3^\circ$ in roll (rotation about velocity vector) and in pitch (oscillations about the spin axis) and $\pm 4^\circ$ in yaw (oscillations about an axis 90° to the velocity vector and in the plane of the orbit). During the time that the satellite is in the earth's shadow, the yaw oscillations build up to $\pm 5^\circ$, while the other two remain about the same. Since the antenna pattern at most of the frequencies is much larger than the magnitude of these oscillations, they have little effect of the data. The effect of yaw motions is to broaden the beam slightly since this causes tip motion and low frequency oscillations of the booms themselves.

At the time of launch, there was some concern as to how the booms would react to the thermal shock as the booms entered the earth's shadow. This was an additional reason

for choosing the retrograde orbit, since it would provide 100% sunlight for the longest period of time. However, from the available spacecraft attitude data, it now seems evident that the satellite experiences almost no additional oscillations caused by this thermal shock (Blanchard, 1969).

B. The Vee Antennas

The travelling wave antenna is made by connecting each leg to ground or by inserting a resistor an odd fraction of a wavelength from the tips of the legs as is done in RAE. Either way the receiver does not see a standing wave even though they still exist beyond the terminating resistor. The advantage of the travelling wave antenna is that it suppresses the back lobes causing most of the energy to be placed in the front lobes.

Each leg of the Vees has an insulating splice cut one quarter of the distance from its tip. A 600-ohm resistor bridges the splice. The antenna then acts as a travelling wave system when the length of the antenna beyond the resistor is an odd number of quarter wavelengths.

The booms forming the Vees consist of hollow cylinders 1.3 cm in diameter. They are made of strips of 0.05 mm thick precision rolled beryllium copper strips. The details of the design, construction and deployment of these booms can be found in the design document for RAE by Mattingley et al. (1970).

One of the major causes of boom distortion is the setting up of thermal gradients by the sun illuminating only one side of the boom. This gradient is minimized by perforating the booms, silver plating the outside surface, and coating the inside surface with a coat of highly absorptive black paint. Most of the heat from the sun is reflected by the silver plating. A small percentage, some 10%, is still absorbed by the silver plating. The perforations let approximately 5% of the sunlight illuminate the inside of the shadowed part of the boom, where the black paint absorbs enough heat to equalize the temperature on both sides of the boom.

At the time of the design of RAE, there was very little literature about a travelling wave Vee's antenna pattern and mechanical properties. Several theoretical studies (Duff 1964; Iizuka 1965) were made and experimental models

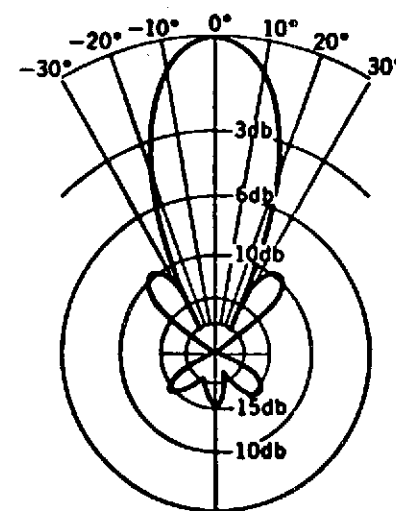
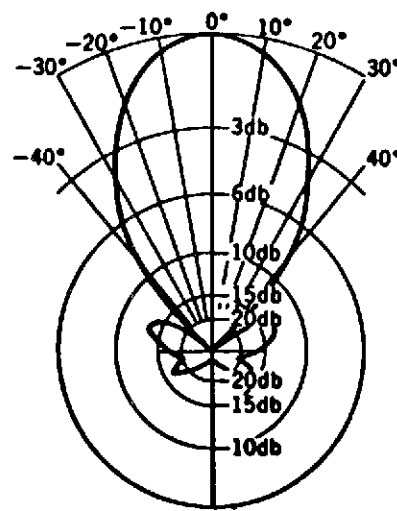
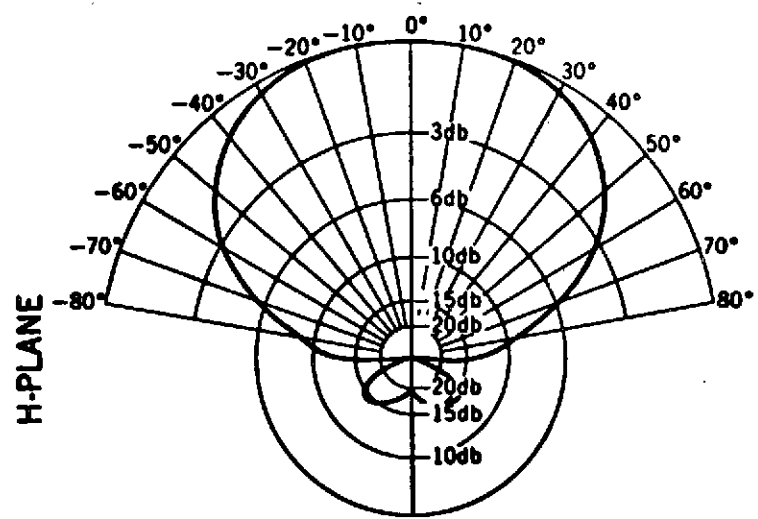
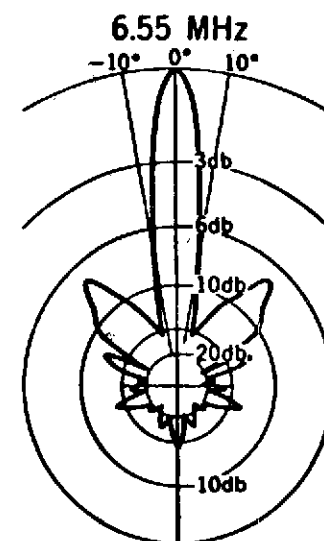
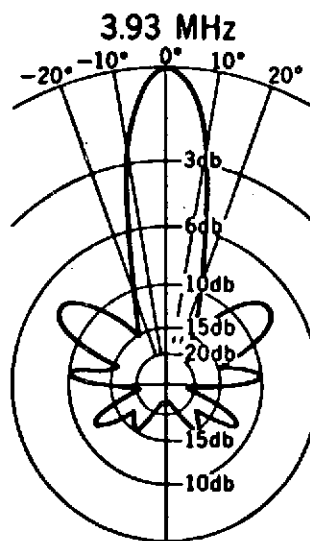
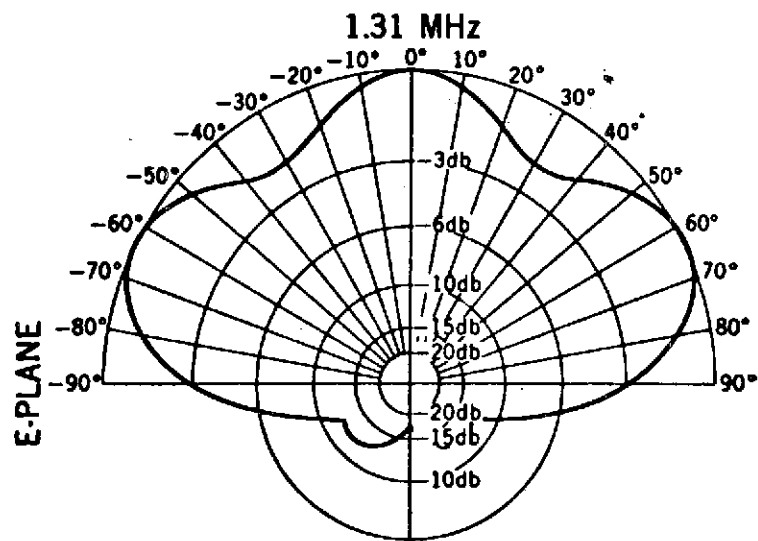
with a scale ratio of 1:100 (Iizuka, 1967) were studied. A series of larger scale models was made by the Collins Radio Company (Collins, 1966) to measure the impedance, current distributions and antenna patterns. These confirmed the theoretical patterns. Figure 3 taken from the paper by WAS shows the antenna patterns for 1.31, 3.93 and 6.55 MHz.

The beam pattern of the Vee antenna at 3.93 MHz is an ellipse $23^{\circ} \times 52^{\circ}$, whose semi-major axis is normal to the orbital plane. The first major side lobe in the E plane is 7 db down and about 50° from the center of the beam. In the H plane, the first side lobe is 17 db down and about 65° from the center. At this frequency the efficiency of the main beam is about 50%.

At 6.55 MHz, the elliptical main beam has narrowed to $14^{\circ} \times 34^{\circ}$. The first major side lobe for this frequency in the E plane is about 7 db down and about 40° away from the center of the beam. In the H plane, the first side lobe is nearly 10 db down and about 40° away from the main beam. The main beam efficiency at 6.55 MHz is also approximately 50%.

Figure 3. - Antenna pattern of the Vee antenna for 1.31,
3.93 and 6.55 MHz. Taken from Weber, Alexander,
and Stone, 1971, Radio Science, 6, 1085.

RAE V ANTENNA PATTERNS



Every 346 days, the antenna beam will have rotated through 90° because of orbital precession. Thus a part of the sky common to two scans 346 days apart will see the beam oriented in orthogonal directions. If the data are properly averaged together, the effective beam will tend to become roughly circular at the larger dimension, and the data will be smeared somewhat. However, as will be discussed later, the averaging may be uncertain.

C. Receivers on the Upper Vee

The receivers to be used with the upper Vee were designed to meet the following requirements: (Somerlock and Krustins, 1968).

1. Measure the signal level to a relative accuracy of $\pm 1/2$ db
2. Respond to a 60 db range of signal levels centered on an antenna temperature of 10^6 K
3. Measure over a decade span of input frequencies
4. Operate for approximately one year in a space environment
5. Maintain or check calibration during their lifetimes

6. Use little power or spatial volume.

The most stringent requirement was that it should make stable precise measurements unattended and because of this requirement a feedback Ryle-Vonberg radiometer (Machin, Ryle and Vonberg, 1952; Somerlock and Krustins, 1968) was chosen. This instrument measures antenna signal strength by a continuous comparison with an internal voltage-controlled noise source, which is adjusted by a servo loop to equal the antenna signal. Because this system measures by a null technique, it is insensitive to internal changes in system gain or bandwidth.

To ensure that the noise source remains properly calibrated and that there is some redundancy in the measurement of the noise source output, one modification was made to the standard Ryle-Vonberg system. The standard Ryle-Vonberg receiver measures the voltage controlling the noise source. A stable thermistor-bridge power meter was added to continuously measure the output power directly from the noise source (Somerlock and Krustins, 1968). The antenna noise is then measured in two ways: (1) by telemetering the noise source control voltage (the "coarse" measurement

in the telemetry stream) and (2) by telemetering the output of the thermistor bridge (the "fine" measurement in the telemetry stream). These two outputs are similar except for their time constants and that the bridge measurement is much more stable and precise. The time constant for the "coarse" measurement was chosen to be 0.1 second. A shorter time constant is more useful for the "coarse" measurement because of its environmental temperature sensitivity. The short time constant also emphasizes dynamic measurements. The "fine" measurement has a time constant of 0.5 second which was chosen to reduce the statistical noise superimposed on the output voltage and provide more accurate mapping (Somerlock and Krustins, 1968). A larger time constant would be effected by beam motion across the sky. The noise source used in making the comparison with the antenna signal is a solid state noise diode. It is unfortunate, that after about nine months of operation, the reed relays in the thermistor bridges failed. However, the "coarse" measurement of the antenna power through the voltage of the noise source has continued.

The sensitivity of a receiver is normally defined in terms of the RMS statistical noise on the output of the receiver. It is given by

$$\frac{\Delta T}{T} \approx \left(\frac{\pi/2}{B\tau} \right)^{1/2}$$

where B is the bandwidth of 40 kHz and τ is the time constant, T is the antenna temperature and ΔT is smallest measurable change in antenna temperature. However, in RAE-1, the receiver is sampled at a slow rate, once a second for the coarse measurement and once every four seconds for the fine measurement. Consequently, the peak of the statistical noise is a better measure of the receiver's sensitivity than the RMS value. This peak noise sensitivity is $\approx 4\%$.

The radiometers operate at 9 frequencies; 0.45, 0.70, 0.90, 1.31, 2.20, 3.93, 4.70, 6.55 and 9.18 MHz. Each frequency has a completely separate local oscillator and tuned-RF first-stage amplifier. Only one RF amplifier is on and in use at any one time. This method gives fewer spurious responses, lower probability of cross modulation between frequencies, and some element of redundancy, since

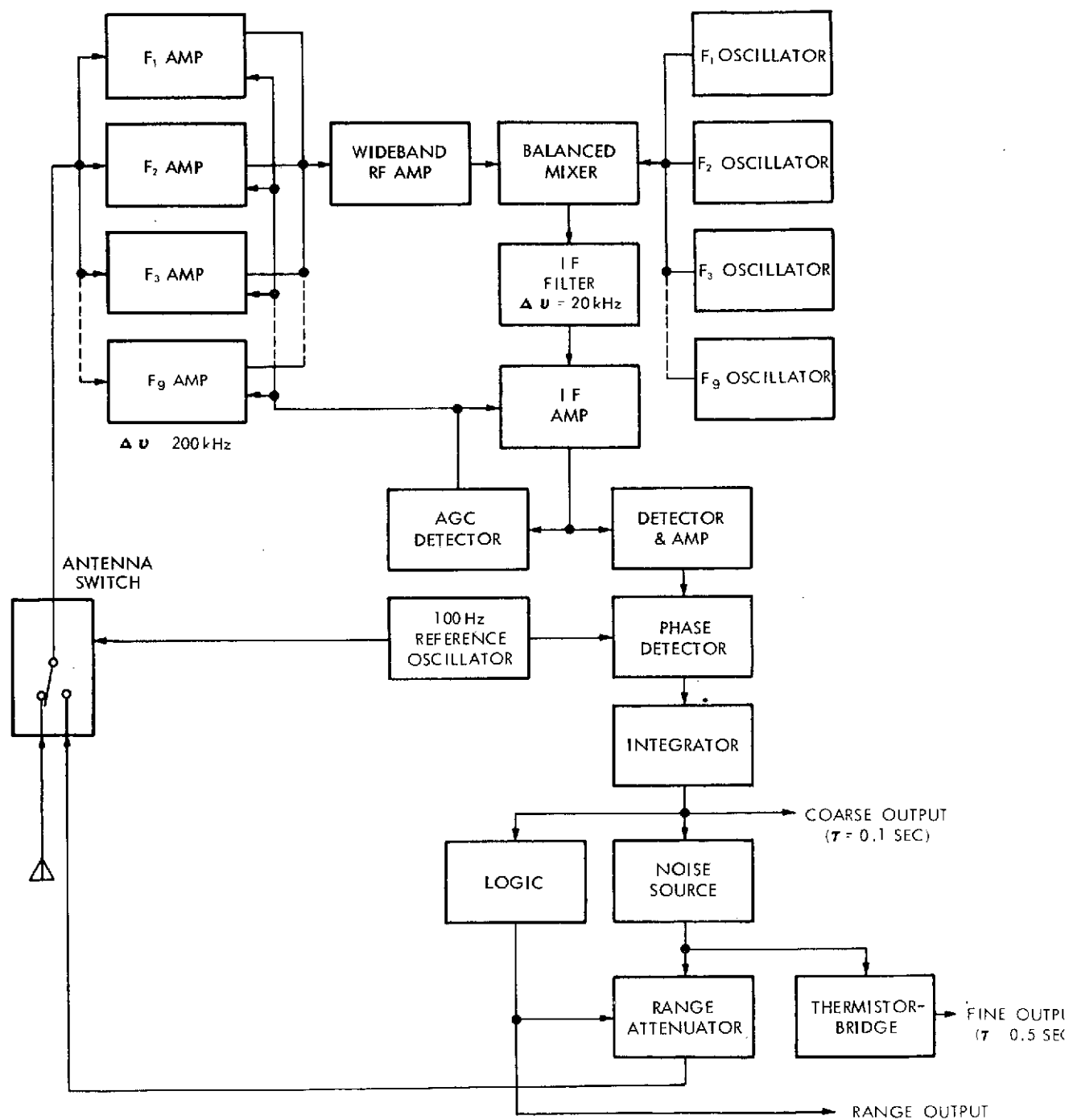
by having independent RF stages for each frequency, should one RF stage be lost only the one frequency is lost, rather than the entire radiometer.

Basically each radiometer consists of a Dicke switch, three amplifiers, a phase detector, integrator, noise source and a thermistor power meter. Figure 4 is a block diagram of the Ryle-Vonberg receivers, taken from the paper by Somerlock and Justins (1968). This technical note has a complete description of the design and operation of the radiometers.

The Dicke switch is driven by a 100-Hz oscillator and alternatively feeds first the antenna signal then the internal noise source into the first RF amplifier stage with a band-pass of 200 kHz. The signal is further amplified by a second wideband RF amplifier before being mixed with the local oscillator and passed through the IF filter (bandwidth of 20 kHz) and amplifier. Because the system is a zero IF system, the effective bandwidth of the system is 40 kHz.

The phase detector and integrator compare the internal noise sources with the antenna signal. They adjust the

Figure 4. - A block diagram of the Ryle-Vonberg receivers used on RAE-1. Taken from Somerlock and Krustins, 1968, "A Precision Spacecraft Radiometer for Hectometer Wavelengths", NASA Tech Note TND-4634.



voltage controlling the noise source until the noise source signal and the antenna signal have the same strength.

The thermistor bridge power meter is an addition to the standard Ryle-Vonberg system. It continuously measures the output power from the internal noise source. Its addition was to insure the accuracy of the measurements of the antenna signal and to provide redundancy by telemetering two independent measurements of the internal noise source. It has a similar feedback system to that of the receiver except that the comparison is made against a dc reference resistor. This allows the meter to automatically compensate for changes in the environmental temperature.

The thermistor bridge has a dynamic range of only 20 db. To attain the desired 60-db range, an attenuator of either 0, 20 or 40 db is inserted before the phase detector. The selection of attenuator is made by two triggers, which sense when the antenna signal is out of range and then cycle through the three attenuators until the antenna signal is within the thermistor bridge's dynamic range. The number of the range attenuator (either one, two or three) is included in the telemetry stream.

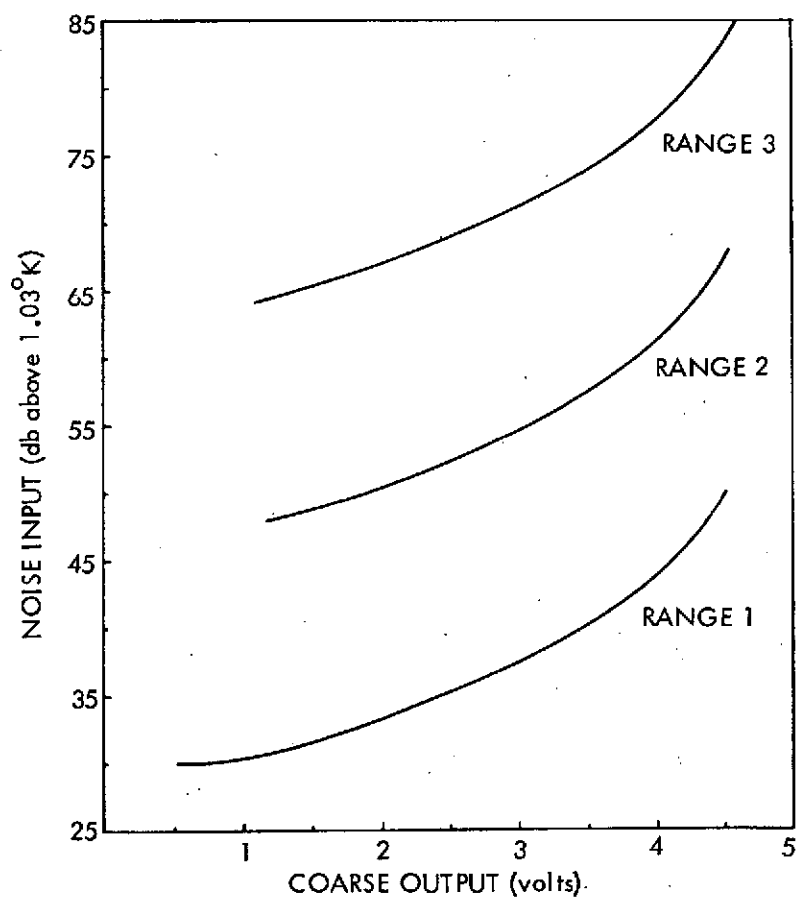
The voltage controlling the noise source is telemetered as the "coarse" readout and the output of the thermistor bridge is telemetered as the "fine" readout.

D. Calibration Procedures

The Ryle-Vonberg radiometers were calibrated while the satellite was in its thermal-vacuum test at Goddard. Each radiometer was stepped through its entire 60 db range in 1 db steps for each of three environment temperatures, 60, 25 and -20°C . The output voltage data of the two receivers were then sorted by receiver, range attenuator setting and temperature and plotted as a function of input noise level.

Figures 5a and 5b (Somerlock and Justins, 1968) are sample calibration curves for the radiometers. Figures 6a and 6b (also from Somerlock and Justins 1968) show the effects of environmental temperature on portions of these calibration curves. The maximum variation of the thermistor bridge's output is $\pm 1/2$ db over a temperature range of 80°C , but note that the variation of the course readout with temperature is much larger for a given input level. For each of the three temperatures (60, 25 and -20°C), the

Figure 5. - Typical calibration curves for (a) the coarse output and (b) the fine output. Taken from Somerlock and Krustins, 1968, "A Precision Spacecraft Radiometer for Hectometer Wavelengths", NASA Tech Note TND-4634.



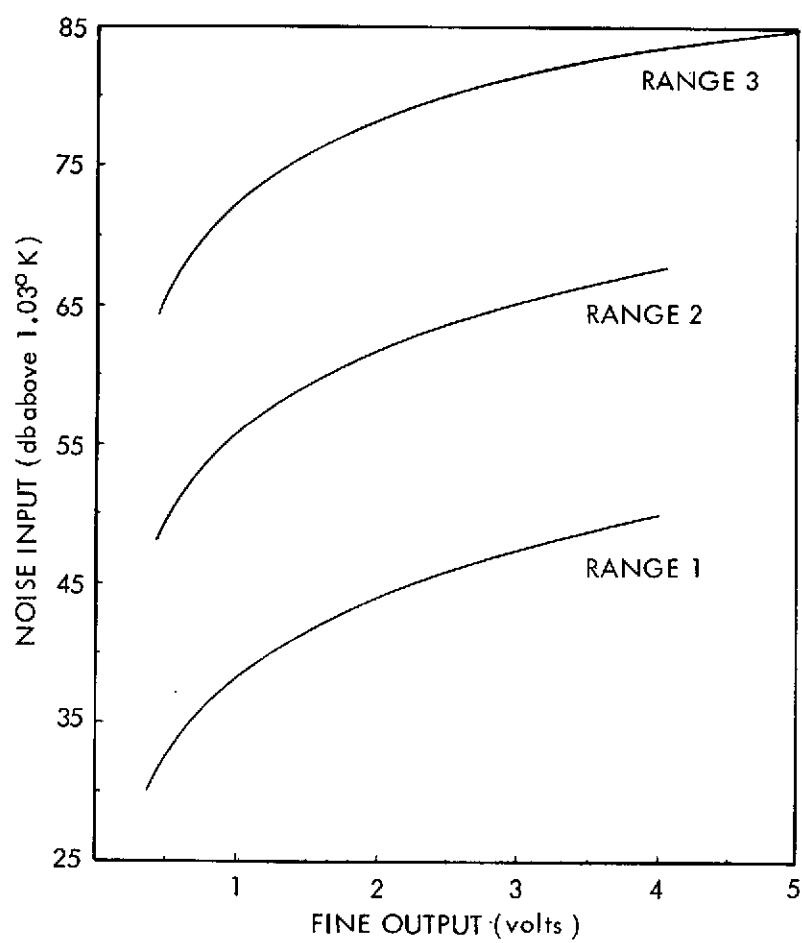
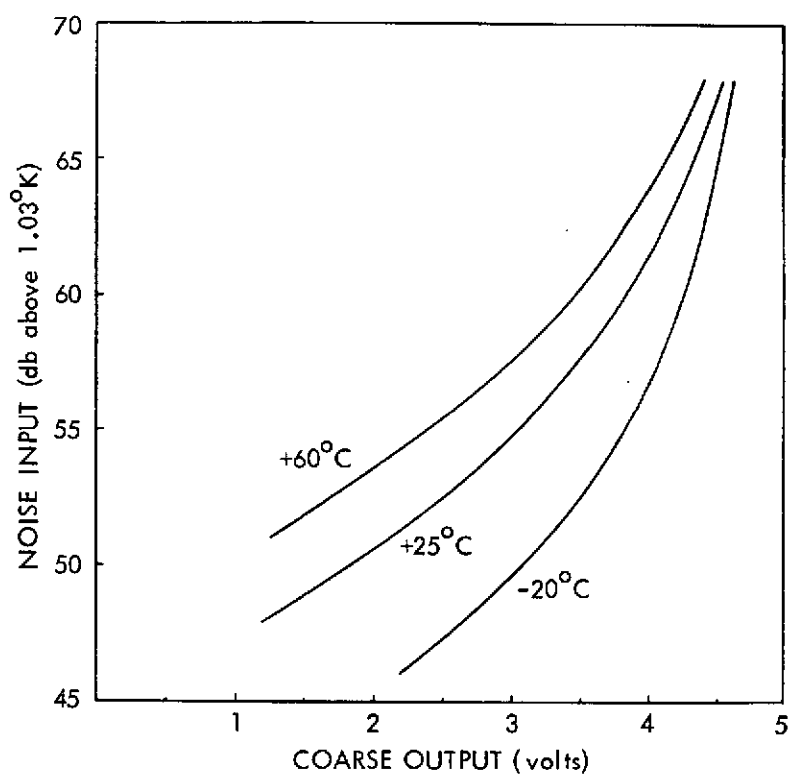
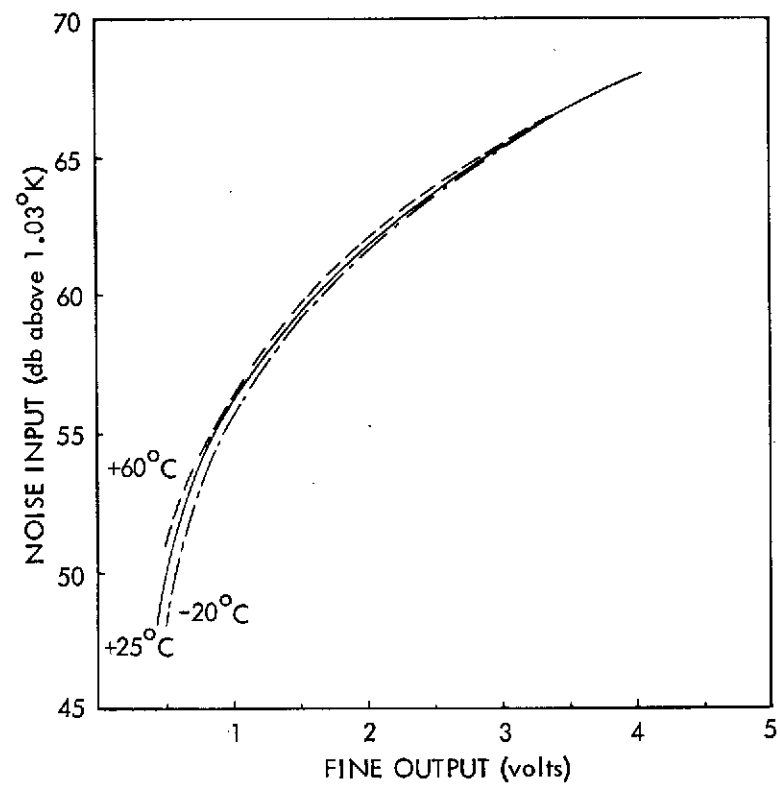


Figure 6. - Examples of the variation of the output with environmental temperature for (a) the coarse output and (b) the fine output. Taken from Somerlock and Krustins, 1968, "A Precision Spacecraft Radiometer for Hectometer Wavelengths", NASA Tech Note TND-4634.





calibration curves for each frequency for each range attenuator setting have been fitted with a fifth degree polynomial for computerizing the calibration of the telemetered data.

A summary of the errors of the calibration procedures is found in Table 1, taken from WAS. In addition to these errors, the error in determining the antenna temperature due to the uncertainty of the fifth degree polynomial fit to the calibration curves, and to the temperature correction is estimated to be ± 0.3 db. The uncertainty in the telemetry resolution is ± 0.2 db. Hence, the total uncertainty is ± 0.6 db or 14% (WAS). This then was the uncertainty in the data at the time of launch. An additional uncertainty is present, if the receiver should suffer instabilities or long term drifts, as will be discussed later.

E. The Telemetry System

The telemetry system consists of a pair of redundant clock and encoder systems, a tape recorder (which failed a few months after launch), and high and low power transmitters. The two separate clock and encoder systems can be cross

TABLE 1. ERRORS IN ABSOLUTE CALIBRATION OF RADIOMETERS

Absolute calibration of standard noise source	± 0.2 db
Calibration of high level noise source against laboratory standard	± 0.05
High level noise source stability	± 0.01
Remotely controlled attenuator calibration	± 0.2
Measurement of dummy antenna insertion loss	± 0.15
Measurement of dummy antenna impedance	± 0.3
probable error	± 0.44 db

coupled so that either clock may drive either encoder. Real time data (directly from the encoder) is transmitted at 400 bits per second using the low power transmitter.

The telemetry system cycles through a sequence covering 154 frames in 9.86 minutes of time. The first 10 frames contain the calibration data. The remaining 144 frames consist of 8 cycles of 18 frames each which contain, among other things, the Ryle-Vonberg (RV) receiver data. Each frame contains four coarse readings and one fine reading from one of the two receivers connected to the upper Vee. With each output is a word identifying the range attenuator used to make the measurement. Each frame also has another word identifying the frequency of the measurements. There are a total of eight coarse and two fine measurements for each frequency, spanning two adjacent frames or eight seconds of time.

The receivers start their cycle at 9.18 MHz and every eight seconds (or two telemetry frames), step down to the next frequency. After observing at 0.45 MHz, the cycle returns to 9.18 MHz. Each frequency is sampled every 72 seconds.

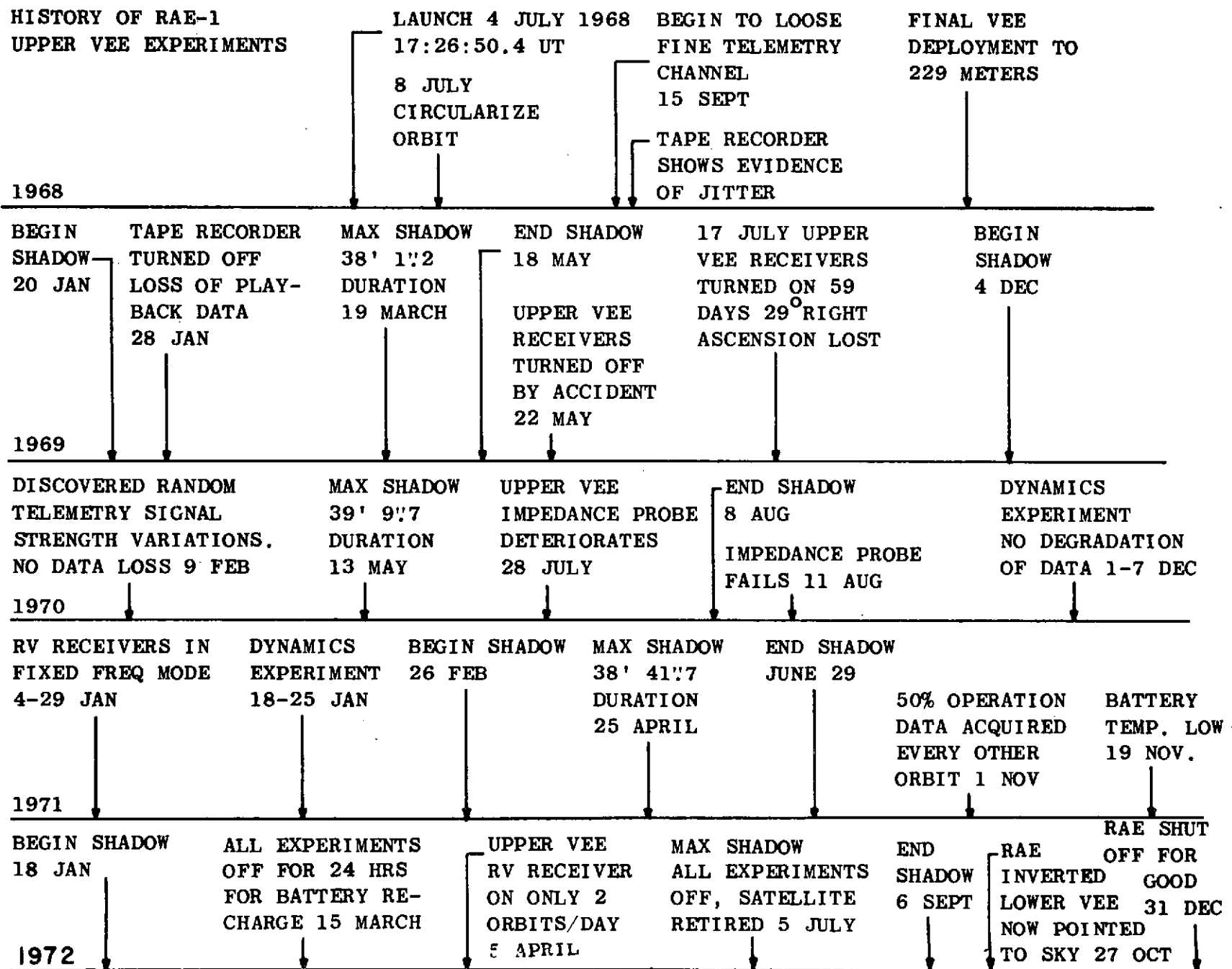
F. System Reliability

The design lifetime of the satellite was for a minimum of one year of operation. RAE-1 has now been operating for over four years with only a few failures. The failure of the tape recorder caused a loss of about 5% of the data. The most serious failure has been the loss of the RV's "fine" telemetry channel, removing the most stable means of measuring the antenna noise power. This failure has been traced to two reed relays in the thermistor bridge power meters and RAE-B has been redesigned to use solid state switches. This failure drastically affects this study, since it has forced the use of the coarse measurement, which as will be shown later, is seriously affected by environmental temperatures.

Figure 7 is a schematic time line of the major events for RAE-1. Only the events affecting the upper Vee antenna are shown. Shadow periods are marked with a heavy line and the duration of the maximum shadow per orbit is shown in minutes and seconds. Except for the 59-day accidental interruption between May 22 and July 17, 1969, data has been

Figure 7. - A schematic time line of the history of RAE-1
showing the major events affecting the upper
Vee experiments.

HISTORY OF RAE-1 UPPER VEE EXPERIMENTS



gathered continuously since the final deployment of the booms in October 1968. From September 15, 1968 to January 28, 1969 the tape recorder deteriorated, eventually causing loss of the playback data. Loss of playback data had a relatively minor effect since approximately 95% of the data in a twenty-four hour period can be transmitted directly to the ground in real time.

The most serious events were the periods of shadow during which the RV receivers apparently suffered instabilities, as will be discussed later.

III. GROUND DATA PROCESSING

Ground data processing can be broken down into three major areas: tracking station processing, the Information Processing Division's telemetry processing, and the Radio Astronomy Branch's scientific processing. The tracking stations are responsible for tracking the satellite, filtering the data, and recording the data on tape in analog form with the appropriate timing standard. The Information Processing Division (IPD) is then responsible for the task of converting the analog tape sent from the tracking station to digital form and converting the digitized data into scientific units (i.e. antenna temperature in units of 10^{-6} K, etc.). The Radio Astronomy Branch is then responsible for the final scientific processing to present the data in summarized form (i.e. maps, spectra, etc.).

A. Tracking Station

There are twelve tracking stations located around the world that are nominally assigned to record RAE-1 data (Ferris and Shea, 1968). Of these, seven are capable of real time

re-transmission of the data to Goddard as required by the project for "quick-look" analysis. Data are recorded at the station on an analog tape along with Greenwich Mean Time (GMT). These tapes are mailed to IPD for further processing and are then archived for permanent storage.

B. Information Processing Division

IPD's function can be broken down into two major steps: digitization and editing of the analog data to convert it to a computer-compatible form and conversion of the data from raw telemetry form to data in scientific units.

Digitization and editing is done on a CDC 3200 with the actual digitization being performed by a special purpose front end on the computer. The computer receives the data on a frame-by-frame basis including the GMT of that frame. The CDC 3200 then utilizes the quality control information from the front end and its own algorithms to eliminate frames with questionable validity. Data that are written on the output tape for further processing have a 99.9% probability of being free of telemetry noise and errors, that is, most of the errors added to the data by the RF telemetry link have

been removed. The amount of data thrown out by the program will vary with the quality of the data. For a tape whose data are clean and free from telemetry noise, it is often less than a dozen frames representing less than 42 seconds of time out of a total duration of 45-60 minutes or about 700-1000 frames. For a tape with noisy data, the programs can throw out as much as 5 or 6% of the tape. Tapes having data with this poor quality or worse are generally deleted from the processing stream entirely. While this means that the data are 99.9% valid and useful, it does not necessarily mean that the data are useful scientifically since no check has been made on the experiment's performance. The program used to digitize and edit the data has been fully documented by Cariga (1971).

The output of the CDC 3200 is then taken to the Univac 1108 for further processing. Here it is merged with orbital attitude data and calibrated (Stewart and Redwine, 1970). The orbital and attitude data contains the positional information for RAE-1. This is merged with the telemetry data, so that each frame is tagged with the pointing position of the upper Vee in the sky.

The 1108 also calibrates the telemetry data. Stored in the computer, in the form of fifth order polynomials, are nine calibration curves one for each of the three range attenuator settings for the three environmental temperatures of 60, 25 and -20°C . Using the set of three appropriate curves for the proper receiver, frequency and range (all three are parameters in the telemetry stream), the decimal value of the RV's antenna output voltage is converted to three input noise temperatures, one for each of the three environmental temperatures used to calibrate the RV receiver. These three antenna temperatures are then fitted with a quadratic curve to represent the variation of the antenna temperature with environmental temperature. The fitted quadratic curve is then used to interpolate between these three temperatures using the actual environmental temperature in the telemetry data.

Four days of RV equivalent antenna temperatures (that is the antenna temperature equivalent to the input noise power as computed from the above procedure), in chronological order, are written on a tape for shipment to the Radio Astronomy Branch. With each measurement is the receiver

identification, the GMT, and the position of the upper Vee in right ascension and declination.

C. Radio Astronomy Branch Processing

There are three main programs, entitled Histogram, Boxave and Con5x5, that are used by the Radio Astronomy Branch to analyze the RV data (Kaiser 1972). The Histogram program produces a histogram of the antenna temperatures in one four day group or file of data. The Boxave program combines the four-day group and merges the data onto a history tape for sky mapping purposes. Con5x5 is a contouring program designed to contour the data on a history tape produced by Boxave.

Histogram combines four days of data into one mean orbit. This can be done since the precession rate is sufficiently small. In four days the orbit moves only 2° , which is within the pointing uncertainty of $\pm 3^{\circ}$. It then separates the data into intervals of 5° of mean anomaly for this mean orbit. This interval was chosen to be small compared to the beam width and to optimize computer useage. A histogram of antenna temperatures is then produced for each

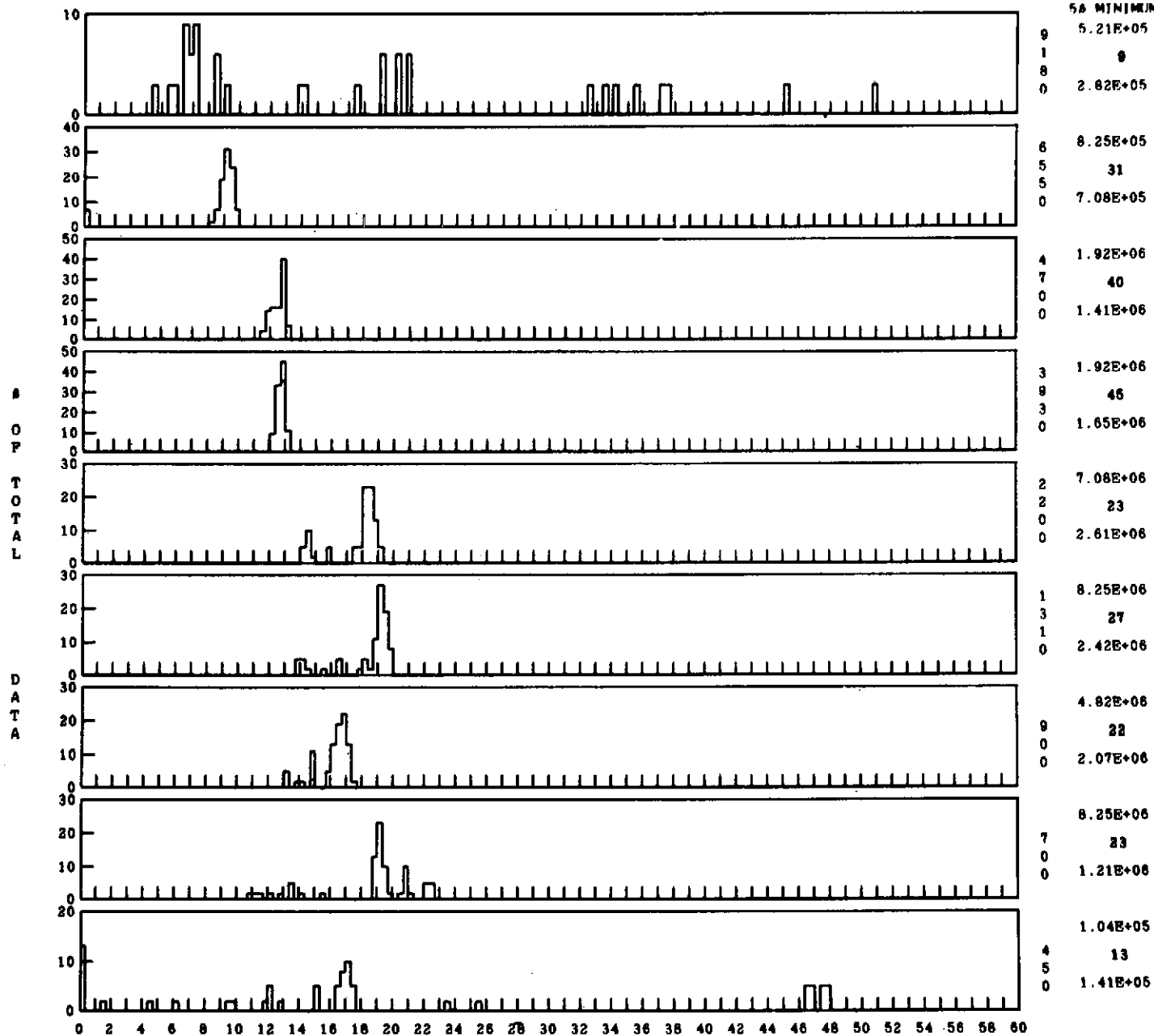
5° interval. The resolution of the histogram is $1/3$ db in calibrated antenna temperature. A sample is shown in Figure 8. Along with the plot each histogram the mode of the histogram, the percentage of points in the mode and the calibrated antenna temperature of the first interval with more than 5% of the data are listed.

After the data for the last 5° interval of mean anomaly has been plotted, two summary plots are made. These are plots of the mode of the histogram vs mean anomaly and of the first interval with more than 5% of the data vs mean anomaly. Following the two summary plots is a table listing GMT, LMT, right ascension, declination, galactic latitude and longitude, geographic latitude and longitude, and geomagnetic latitude and longitude as a function of mean anomaly.

Boxave is an averaging program whose final output is a history tape and a printout of the history tape. It first filters the data in an attempt to remove interference. The averaging is then done in a matrix on the sky of $5^{\circ} \times 5^{\circ}$ boxes. The size of the boxes was chosen to optimize computer core usage and computer through-put. It has provision to accumulate a history of many runs in this matrix, processing

Figure 8. - A sample of the histogram program's output.

UPPER V

DATA DISTRIBUTION IN 10-15 MEAN ANOMALY INTERVAL.
700107 TO 700110MODE
PER CENT
5A MINIMUM

DB ABOVE 100000 DEGREES KELVIN IN ONE THIRD DB INTERVALS

from one to four files in four-day groups. Unlike the histogram program, it works only on one specified frequency at a time.

The program first passes the data through two filters. The first filter is a window of a specified width in decibels centered over a specified background temperature, e.g. a window of ± 2.0 db width centered on a temperature of one million degrees. Data within this window are kept and all the other points are removed. This removes a large part of the effects of solar type III bursts, ground breakthrough, and plasma emission from the data. The width and center temperature of the window must be chosen with care so as to throw out only the undesirable data. In practice their values are the final result of an iterative procedure. Usually a first run is made through a tape with a fairly wide window centered on a calibrated antenna temperature that is determined by an examination of the raw data. The average of the first pass is used as the center temperature of the window for a second run through the tape with a narrower window. The process is repeated until the average calibrated antenna temperature converges. The width of the window is set to a

value chosen by examination of the raw data to remove undesirable data but still wide enough to allow for the expected variation of the galactic background about the average. Practice has shown that only two iterations are necessary. Obviously the data are added to a history tape only on the last step while the previous steps use only a dummy history tape.

The second filter examines ten minutes of data for continuity. Only data that does not have any step-like variations in it is kept.

Any data points surviving the two filters are placed in a matrix of $5^{\circ} \times 5^{\circ}$ boxes in right ascension and declination. Each time 30 points are accumulated in a $5 \times 5^{\circ}$ box, the program computes an average and a standard deviation. It removes any points that are 4σ above or below the average. It then re-computes the standard deviation and continues to throw out points until all the points are within 4σ of the average. Should the number of remaining points fall below a specified minimum level, such as ten, the entire set of data in the box is thrown out. If the set of 30 points is well behaved, that is, the galactic background is well

defined, the process converges very rapidly and usually only one or two iterations are necessary. If the data are not well behaved, the process does not converge and the end result is the loss of all the points within the thirty point set. The results are saved in the form of the summation of the calibrated antenna temperatures within the box (ΣT_i), the summation of the calibrated antenna temperature squared (ΣT_i^2), and the number of data points within the box (N).

After the program finishes the input tape, it then reads the history tape. The history tape contains a $5^\circ \times 5^\circ$ matrix of the sky for each frequency and receiver. Each matrix element contains ΣT_i , N, and ΣT_i^2 , from previous runs. The program merges this run's results into the matrix and then re-writes the matrix back on the history tape. There is a provision in the program to use a dummy history tape so that no actual history tape is saved and the matrix developed contains only the data from the current run.

The matrix is then printed. With each $5^\circ \times 5^\circ$ box, the program prints the average antenna temperature, the standard deviation, and the number of points for that box. A sample of Boxave output is shown in Figure 9.

Figure 9. - A sample of the Boxave program's output.

AVERAGE TEMPERATURE (TIMES 1E 06)
STANDARD DEVIATION (PER CENT OF AVERAGE)
NUMBER OF AVERAGED MEASUREMENTS

UPPER V ANTENNA 3930 KHZ

DECLINATION

60	I		I	0.76	I		I		I		I		I		I		I
70	I		I	8.0	I		I		I		I		I		I		I
55	I		I	13	I		I		I		I		I		I		I
55	I	0.74	I	0.71	I		I	0.72	I	0.80	I	0.89	I		I		I
70	I	5.4	I	7.4	I		I	8.2	I	9.0	I	9.6	I		I		I
50	I	156	I	50	I		I	17	I	38	I	13	I		I		I
50	I	0.85	I	0.82	I	0.72	I	0.71	I	0.78	I	0.75	I	0.73	I		I
70	I	5.3	I	5.4	I	5.7	I	6.0	I	8.5	I	9.9	I	7.8	I		I
45	I	245	I	239	I	147	I	66	I	13	I	22	I	31	I		I
45	I	0.81	I	0.84	I	0.85	I	0.82	I	0.72	I	0.74	I	0.74	I	0.80	I
70	I	6.7	I	6.1	I	5.4	I	4.7	I	4.8	I	8.1	I	6.5	I	11.1	I
40	I	71	I	187	I	221	I	170	I	86	I	44	I	24	I	45	I
40	I		I	0.80	I	0.83	I	0.87	I	0.84	I	0.74	I	0.73	I	0.70	I
70	I		I	6.6	I	5.1	I	4.9	I	4.9	I	5.0	I	6.1	I	5.5	I
35	I		I	28	I	174	I	209	I	197	I	95	I	99	I	14	I
35	I		I		I	0.77	I	0.82	I	0.89	I	0.84	I	0.74	I	0.74	I
70	I		I		I	5.3	I	5.4	I	5.9	I	5.5	I	4.4	I	5.4	I
30	I		I		I	26	I	138	I	174	I	183	I	101	I	141	I
30	I		I		I		I	0.80	I	0.81	I	0.88	I	0.81	I	0.75	I
70	I		I		I		I	6.7	I	6.0	I	5.9	I	6.3	I	5.0	I
25	I		I		I		I	38	I	173	I	160	I	165	I	106	I
25	I		I		I		I		I	0.82	I	0.78	I	0.86	I	0.75	I
70	I		I		I		I		I	7.4	I	6.8	I	5.6	I	5.5	I
20	I		I		I		I		I	77	I	124	I	170	I	119	I
20	I		I		I		I		I		I	0.82	I	0.78	I	0.84	I
70	I		I		I		I		I		I	5.9	I	6.0	I	5.7	I
15	I		I		I		I		I		I	98	I	143	I	147	I
15	I		I		I		I		I		I		I	0.78	I	0.79	I
70	I		I		I		I		I		I		I	7.4	I	6.7	I
10	I		I		I		I		I		I		I	144	I	161	I
10	I		I		I		I		I		I		I		I	0.78	I
70	I		I		I		I		I		I		I		I	7.4	I
5	I		I		I		I		I		I		I		I	73	I
5	I		I		I		I		I		I		I		I		I
70	I		I		I		I		I		I		I		I		I
0	I		I		I		I		I		I		I		I		I

4.00	3.67	3.33	3.00	2.67	2.33	2.00	1.67	1.33	1.00	0.67	0.33
TO	TO	TO	TO	TO	TO	TO	TO	TO	TO	TO	TO
3.67	3.33	3.00	2.67	2.33	2.00	1.67	1.33	1.00	0.67	0.33	0.0

RIGHT ASCENSION

52

For a four-day group with good data quality the number of data points that will be included in a $5^{\circ} \times 5^{\circ}$ box centered on the group's mean orbit will vary from typically 30 to 100 data points. The standard deviation will generally be less than 10% and often less than 7%, which agrees favorably with the $\Delta T/T$ estimate discussed in Chapter II.

Con5x5 is a contour program that will contour the data on the history tape produced by Boxave. Control parameters are a title, frequency code, maximum and minimum antenna temperatures and maximum and minimum standard deviations, and a set of contours and the minimum number of points. By specifying the minimum number of points, the maximum and minimum antenna temperatures and standard deviations, it is possible to skip over those areas of the sky matrix that are particularly plagued with ground breakthrough since this will show up as a high antenna temperature, a large standard deviation, or a low number of points.

Prior to doing the contouring itself, the program smooths the data. This is done by determining a weighted average of any one box and the four adjacent boxes. The central box has a weight of 50% and each of the adjacent boxes has

a weight of 12.5%. This additional smoothing helps remove small scale variations that could clutter the contour map with a lot of false fine detail.

For astronomical purposes, the usual coordinates are right ascension and declination. It also will plot the contours in galactic longitude and latitude.

IV. THE UPPER VEE DATA

Very early in this research, it was realized that it would be virtually impossible to produce a map for each of the nine frequencies that are operating on the RV receivers. For frequencies below 2 MHz, the antenna pattern broadens considerably, ionospheric plasma problems arise and one begins to depart from the goal of having at least an order of magnitude better resolution than a dipole. Since the antenna was optimized at 3.93 MHz, it was decided to use this as the prime frequency.

Preliminary examination of the 9.18 MHz data indicated that this frequency suffered from too much ground breakthrough to be useful, at least in the first analysis. For 4.70 MHz, the data were essentially a duplication of the 3.93 MHz data. This then left 6.55 MHz as the only logical choice of a secondary frequency, even though initially it was felt that it too might suffer from too much ground breakthrough. Frequencies below 3.93 MHz were ruled out because of the reasons mentioned above. A secondary frequency was believed to be desirable since it give an opportunity for

double checking the methods and the features found in the maps, since those features found in both maps would have a higher likelihood of being real.

The upper Vee is equipped with two identical Ryle-Vonberg receivers, RV1 and RV2. Under normal operating conditions RV2 was on for six days and RV1 for one day of each week. RV1 is considered the normal backup system and was on only once a week to confirm that it was still working until late in 1971 when RV2 was used exclusively.

During the course of this analysis, when it became obvious that RV2 was suffering from some kind of instability, an attempt was made to use RV1 data as it appeared to be more self-consistent. However, there was never enough data in any one time period to allow construction of a reliable map.

Consequently a filter was built into the various programs to permit separating data from the two receivers. The rest of this thesis deals exclusively with RV2. Rejection of the RV1 data results in a loss of only 1/7 of a week's data. The remaining data will quite adequately map the sky with only a small change in the statistics. However, the

converse is not true, there are insufficient RV1 data to make a map. Unfortunately the discovery that RV2 was becoming unstable occurred too late to switch to RV1.

A. Ground Breakthrough

In Figure 2, note the period of intense emission occurring at 00:20-50 GMT. Note that the lower Vee has a higher level than the upper Vee indicating that the source must have been located below the satellite. This has generally been termed ground breakthrough. Herman and Caruso (1972) have shown that this terrestrial interference frequently breaks through the ionosphere at levels ≥ 15 db above the galactic background. This interference is well correlated with thunderstorm activity. In addition to this, there is the ionospheric plasma emission which occasionally reaches as high as 3.93 MHz and overwhelms the galactic background. These two can be distinguished from each other because ground breakthrough first appears at 9.18 MHz and gradually moves down in frequency as the ionosphere becomes more transparent, and ionospheric plasma emissions start at 450 kHz and move up in frequency as the plasma density and hence the plasma frequency increases.

B. Glitches

In Figure 10 at 09:10 GMT is an example of what is termed a "glitch" or discontinuity. These are characterized on the upper Vee by a sudden drop in the calibrated antenna temperature, then being reasonably constant for a multiple of 9.86 minutes, and then having a sudden rise to the "pre-glitch" level of the equivalent antenna temperature. The glitches generally occur simultaneously on all instruments that are running at the time.

The fact that they are generally a multiple of 9.86 minutes (which is the telemetry system's cycle time) in duration leads one to suspect that there is a problem within the spacecraft's subcommutator hardware or within the ground data processing system. Originally it was surmised that the problem was due to misidentification of the receiver, since that particular parameter is examined by the IPD 1108 computer only once in each sequence cycle of 154 frames during the process of converting the telemetry data to antenna temperature. This is somewhat dangerous since two adjacent bit errors in this performance parameter could cause

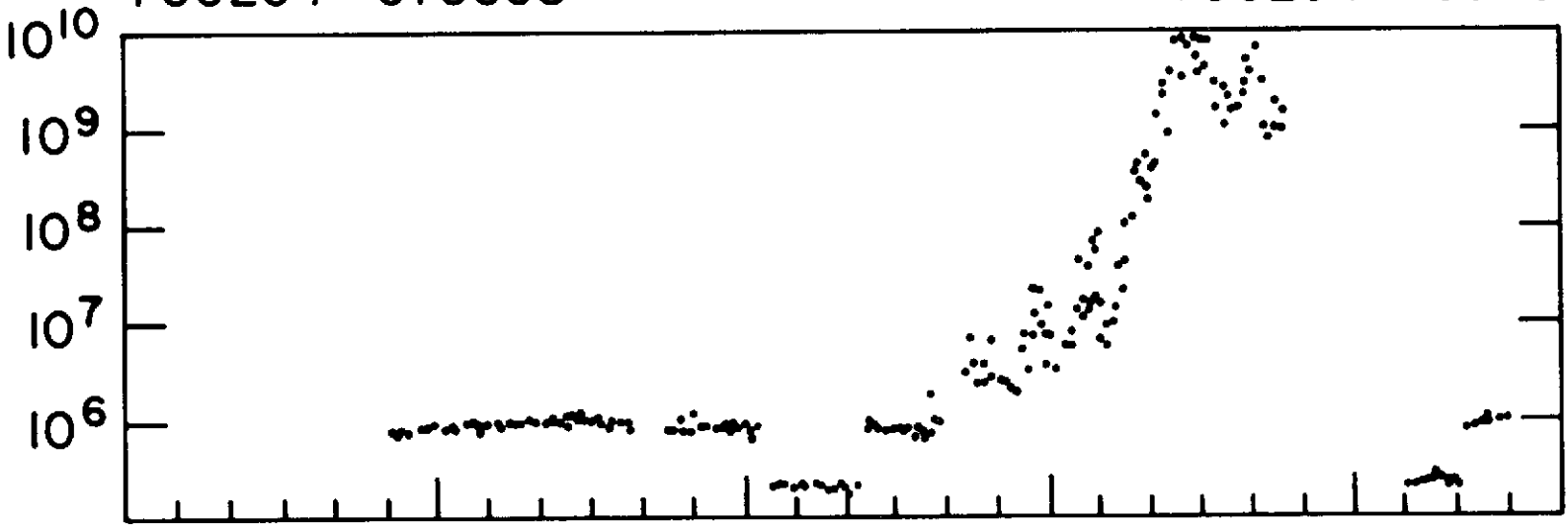
Figure 10. - A sample of raw data for 3.93 MHz showing a
"glitch" at 09:10 Greenwich Mean Time.

FREQUENCY 3.93 MHz

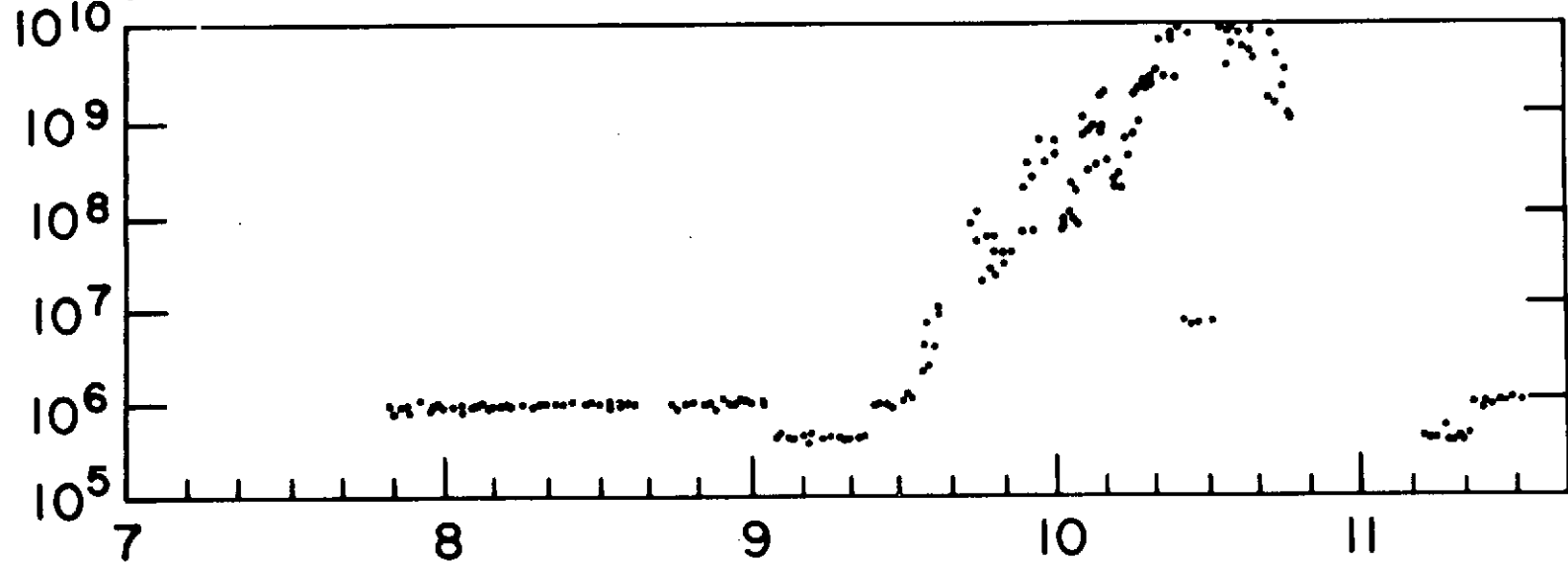
START TIME
700204 075008

STOP TIME
700204 113028

CALIBRATED ANTENNA TEMPERATURE (°K)



UPPER
LOWER



GREENWICH MEAN TIME
IN HOURS

misidentification. It is quite likely to have two adjacent bits in error, since telemetry noise is very bursty.

However, the discovery that the glitch appears in nearly all instruments simultaneously appears to rule out this possibility. The most likely cause now appears to be in the encoders on the satellite. The zero level of the encoders is a performance parameter in the telemetry stream. This is examined by the IPD 1108 computer only once per sequence cycle. Should there be bit errors in the encoder level (particularly in the high order bits), the 1108 will calibrate all of the data erroneously. Similarly, since there are two encoders on board, there might be the same problem occurring as in the mis-identification of the receivers, i.e. bit errors in the parameter in the only frame that the program examines.

All three conditions are caused by not allowing for the possibility of bit errors. All three parameters are the type that, if the data were noise free, need be sampled only once per telemetry sequence. A better method would be to examine all of the readouts of these parameters for each sequence, and then use the most frequently occurring value.

This would greatly reduce the possibility of bit errors giving false information.

Further evidence that these glitches arise from the satellite's on board telemetry system lies in their frequency of occurrence. In the first year of operation, very few of these discontinuities occurred. To the best of the author's knowledge, the first glitch occurred in the fall of 1969. Their rate of occurrence remained roughly constant through 1970 and early 1971, but then began to increase.

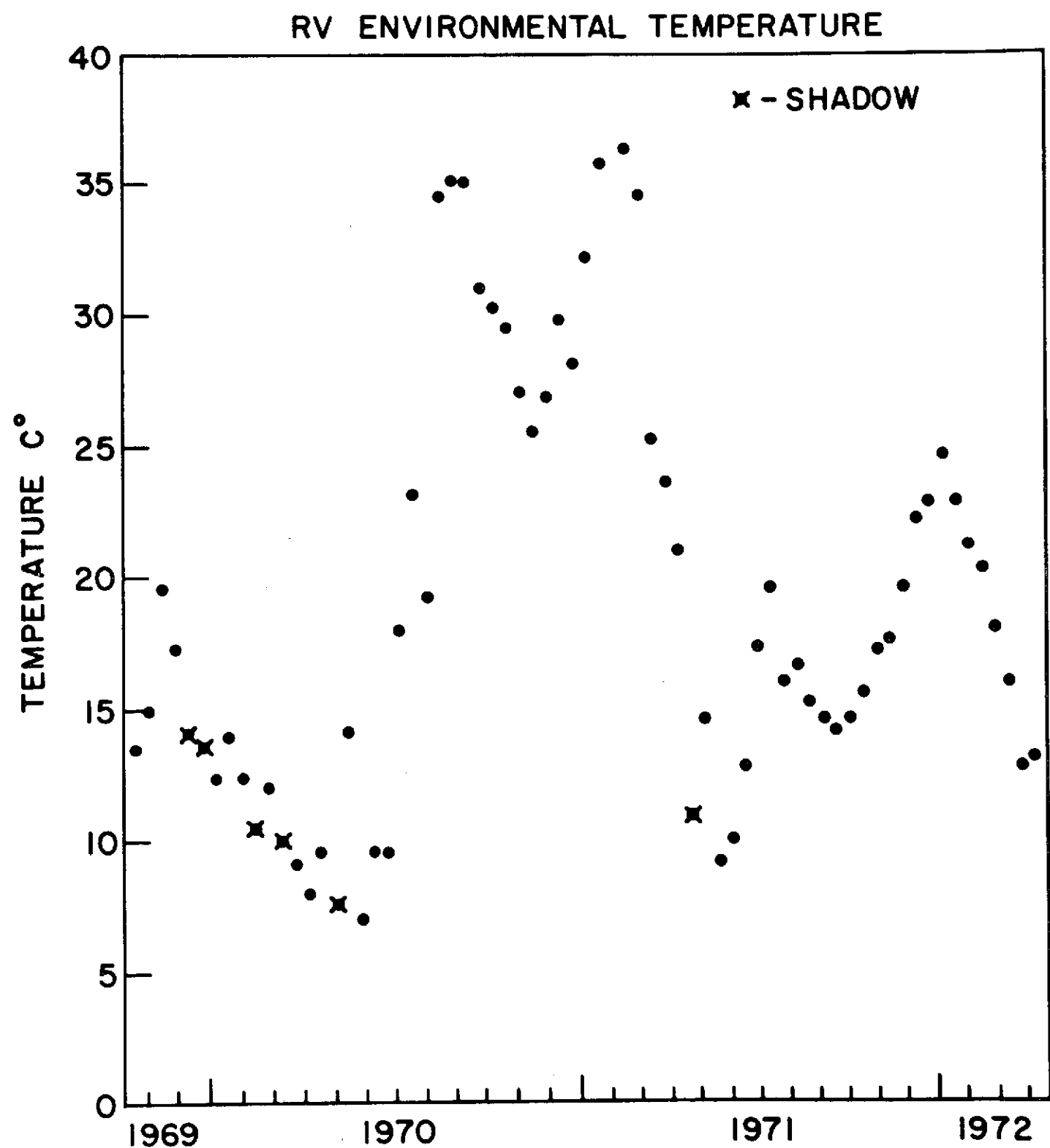
As the various satellite subsystems, particularly the telemetry system and the solar cells, begin to weaken with age, the satellite's signal will tend to become erratic and weaker, increasing the probability of bit errors occurring.

Fortunately these discontinuities are sufficiently sharp that the second filter in the Boxave will eliminate nearly all of them.

C. Receiver Stability

Although the satellite is well insulated, there is still some temperature variation, particularly during the time of shadow periods. Figure 11 shows the long term environmental

Figure 11 - A plot of the long term environmental temperature variation of the RV receivers.



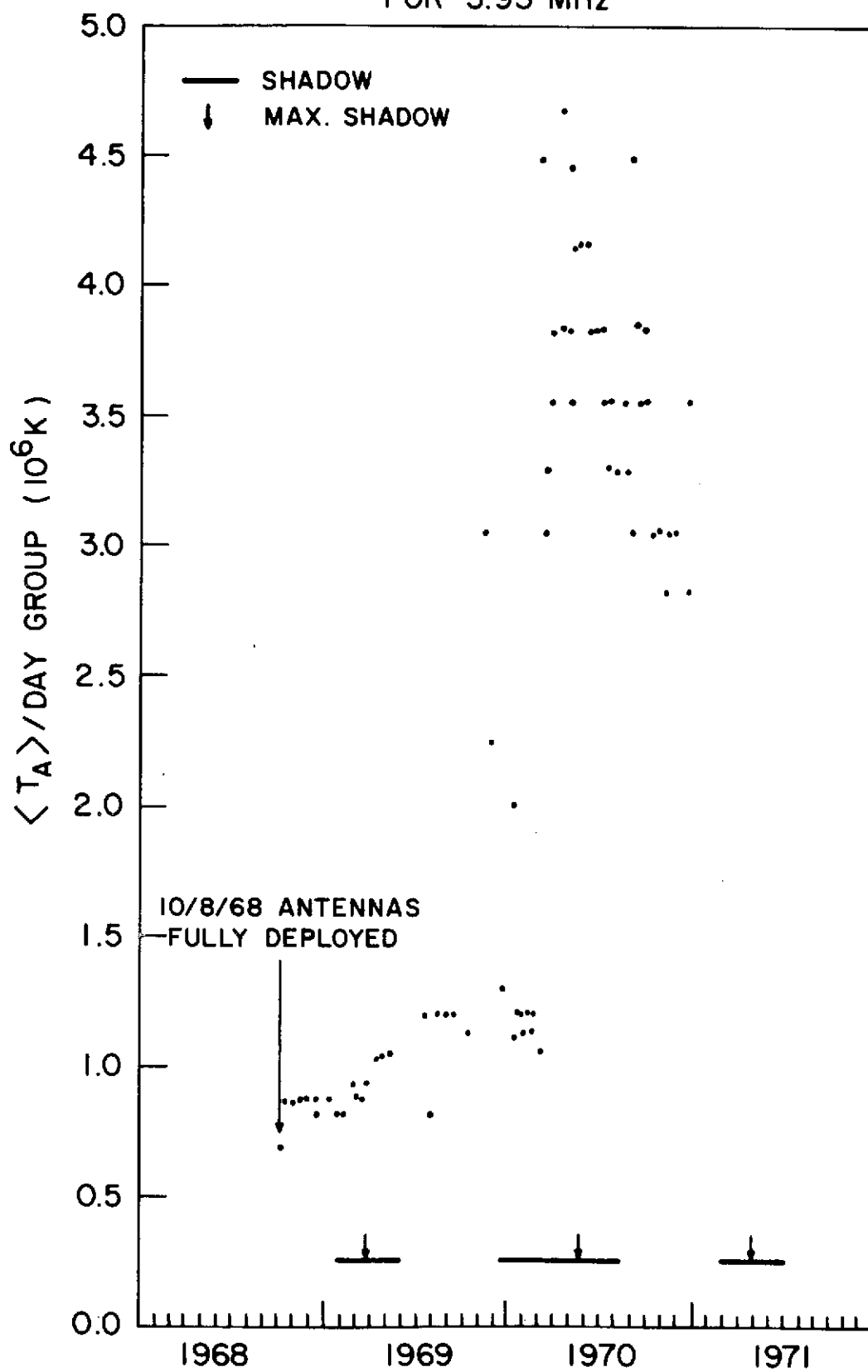
temperature behavior of the RV receivers. Most of the scatter is because the temperatures are not taken at the same place in the orbit, and the range of scatter is an indication of the short-term environmental temperature variations. Note that in March and April, 1970 and May and June, 1971, the satellite was particularly cool. This was during the time of peak shadow duration.

Figure 12a and 12b shows the long term behavior of RV2 at 3.93 and 6.55 MHz respectively. The average equivalent antenna temperature over the entire scan of the sky was taken from the histograms for each four day-group. Problem areas containing ground breakthrough, glitches and plasma noise were ignored so that the average value reflects the receiver's response to the galactic background over an entire four-day group of data. The apparent stratifications are the result of the digitization steps in the histograms.

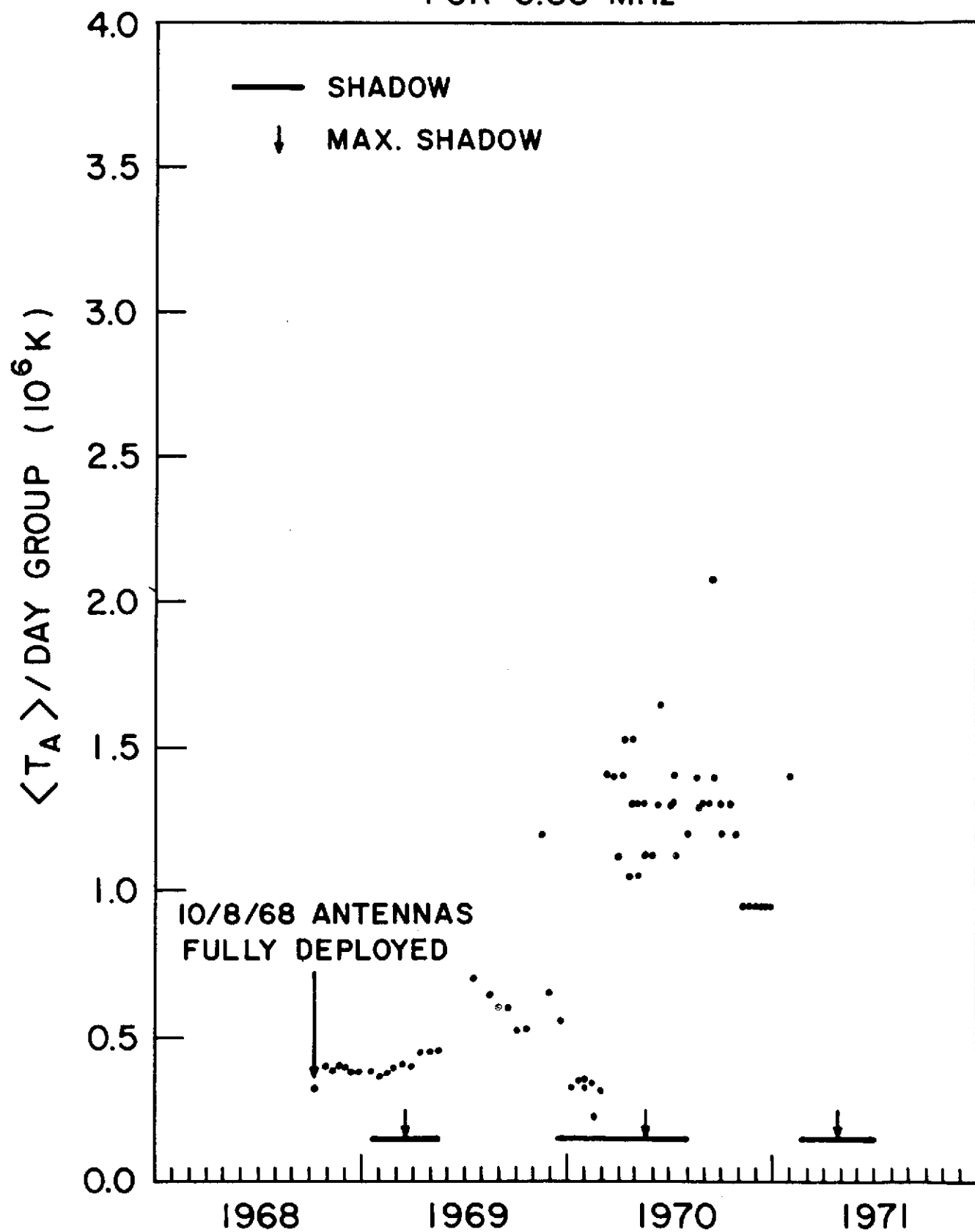
Note that the long term behavior is anything but good, particularly in 1970, where the longest shadow occurred. Referring back to Figure 6a which shows an example of the calibration curves of the course readout, note that the variation of the worse readout at low input noise level is

Figure 12. - The long term response to the galactic background of RV2 at (a) 3.93 MHz and (b) 6.55 MHz showing the receiver instabilities.

AVERAGE ANTENNA TEMPERATURE
FOR 3.93 MHz



AVERAGE ANTENNA TEMPERATURE FOR 6.55 MHz



particularly sensitive to temperature. Unfortunately this is precisely where the galactic background lies.

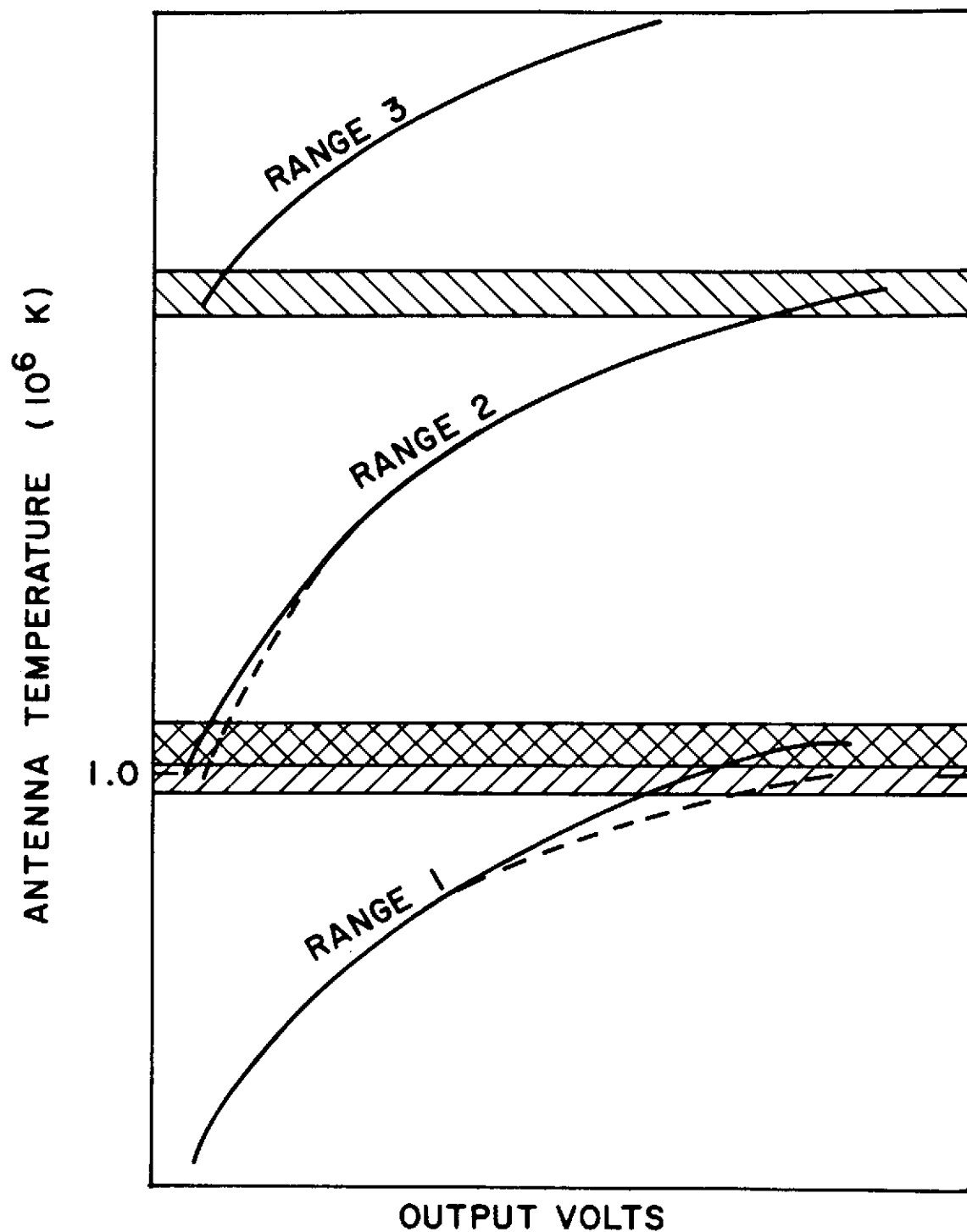
Coupled with this problem is the fact that the receivers were calibrated at only three temperatures of which, in practice, only one was near the range of operating temperatures. With only these three points available, the only curve that could be used to fit the temperatures is a quadratic curve which may not adequately describe the actual temperature variation.



At 3.93 MHz, the receiver was reasonably well behaved until February, 1970. There appear to be two major groups of data, between October, 1968 and March, 1969 and between August, 1969 and February, 1970 that were reasonably consistent. During the first shadow period, March, 1969 - June, 1969, the average calibrated antenna temperature increases steadily from one group to the next.

The behavior after February, 1970 was quite erratic, with the maximum value of the average equivalent antenna temperature reasonably centered about the time of maximum shadow and hence minimum environmental temperature. The very rapid change that took place in March and April, 1970

would appear to be due to a change in the calibration curves of range 2 with respect to range 1. At the time of launch, the galactic background lay just below the region of change from range 1 to range 2 for RV2. This background is represented by the dashed line in Figure 13. In this Figure, the regions of overlap from one range to the next are marked by cross hatching. One possible change in the shape of the calibration curves is shown schematically by the dotted lines in Figure 13. The change in the calibration curve would result in a change in the gain of range 1 with respect to range 2 so that the galactic background now lies in the range change region. The conjectured change in the calibration curves would also result in the low end of the higher range being discontinuous with the high end of the lower range. The equivalent antenna temperature that is measured would vary widely depending on which range the receiver happened to be in at the time of the measurement. This then makes the current measurement dependent on the range the receiver was in at the last time it was sampled. If during a particular time period, one had nearly equal number of measurements in both ranges, one could find things like a bi-modal distribution of antenna temperatures.

Figure 13. - A schematic diagram indicating a possible change in the shape of the calibration curves that could possibly explain the very rapid changes in RV2's response to the galactic background.



- ORIGINAL RESPONSE CURVES
- POSSIBLE NEW RESPONSE CURVES
-  OLD REGION OF RANGE CHANGE
-  NEW REGION OF RANGE CHANGE

The 6.55 MHz data reflect nearly the same behavior, although a tendency to return to the original background levels appears in December, 1969 and January, 1970. But after March, 1970, the average antenna temperature appears to behave as erratically as at 3.93 MHz.

D. Correction for Receiver Instability

From the discussion of the preceding section and the data shown in Figures 12a and b, it would appear that no reasonable analytic curve could reproduce the receiver changes at either frequency for a majority of the data.

At 6.55 MHz, one can use the data from October, 1968 through April, 1969 without correcting for receiver instability. By choosing the appropriate data and an analytic expression for the drift, one could extend the data through February, 1970. However, the resultant map would be rather spotty, since a fair amount of the data in the last six months of 1969 could not be used.

The same comments generally hold for 3.93 MHz, except that there appear to be two time periods (October, 1968 through March, 1969 and August, 1969-February, 1970) that

could produce two maps without receiver drift becoming a problem. By using the proper curve and carefully choosing the data to be used, these two time periods could be used to produce one map.

Because most of the data could not be used with any reasonable analytic expression of receiver drift, I chose a simpler method to remove this instability. At each frequency, I specified a standard background antenna temperature based on the period from October, 1968 through February, 1969, when the receivers were stable. This level was chosen as the value of most of the modes of the histograms for this time period. These values are marked with arrows in Figures 12a and 12b and are 0.89×10^6 and 0.38×10^6 K for 3.93 and 6.55 MHz respectively.

For each four-day group in 1970, the average equivalent antenna temperature, deleting the problems such as ground breakthrough or plasma emission, was determined for both frequencies from the modes of the histograms for the entire scan across the sky. The ratio of this average to the standard value was used to normalize the four-day group to the pre-defined level. This presupposes that the average

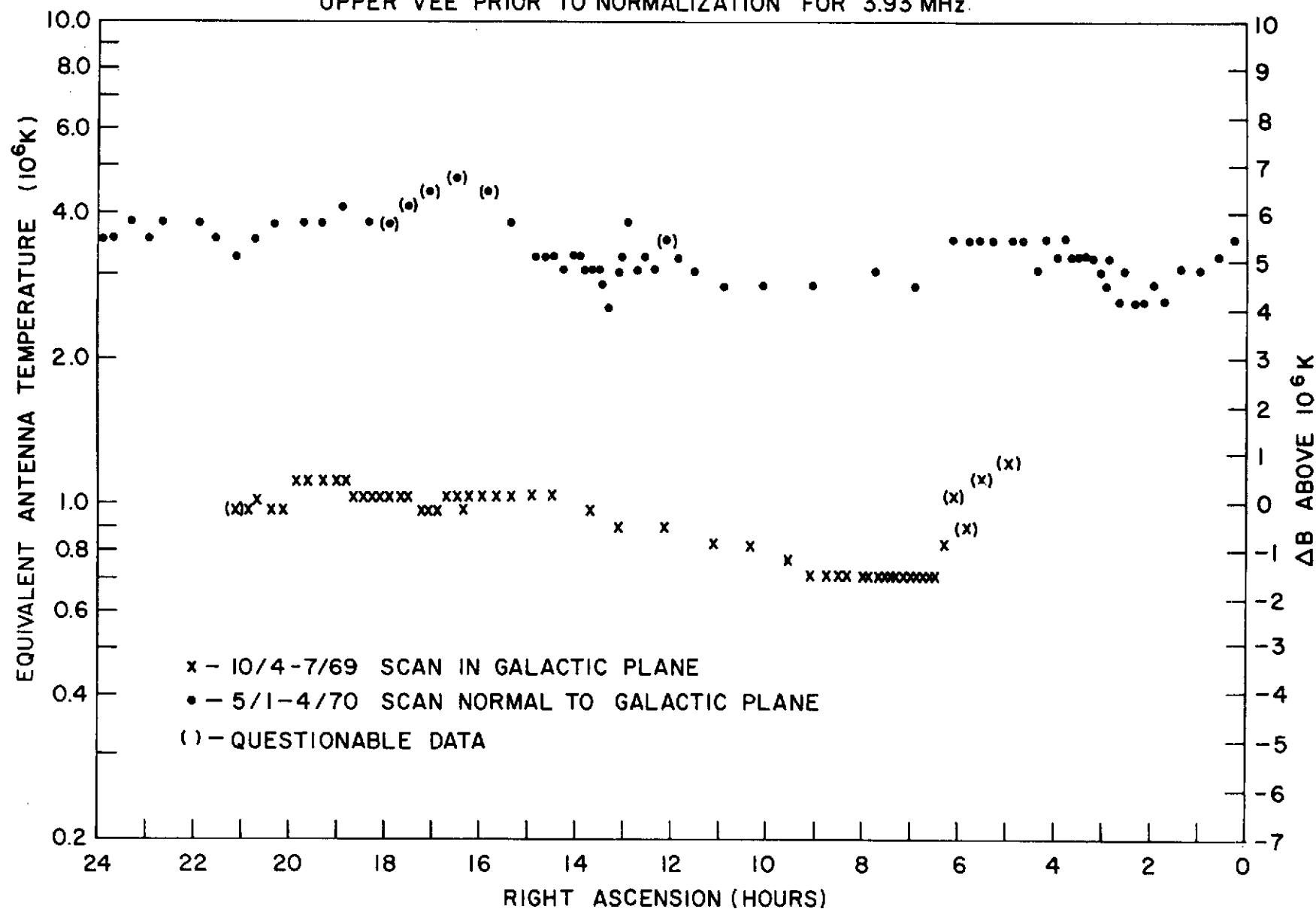
equivalent antenna temperature is independent of the orientation of the antenna's scan across the sky to within reasonable limits.

The raw data shows the necessary low contrast. Figure 14a is a plot of the equivalent antenna temperature (not normalized) as a function of right ascension for 3.93 MHz. The scan labeled 10/4-7/69 is in the galactic plane and the scan for 5/1-4/70 is normal to the galactic plane and passing near the galactic poles. The large difference in equivalent antenna temperature is due to the receiver instabilities that occurred in late 1969 and early 1970. The equivalent antenna temperature is plotted on the left hand scale as the logarithm of the temperature in units of 10^6 K and on the right hand scale as decibels above 1×10^6 K. Figure 14b is a similar plot for 6.55 MHz. In both frequencies the contrast is low for the two scans. The plots indicate that a window of ± 2 db centered on the appropriate background level will pass all of the galactic background and a minimum amount of the interference.

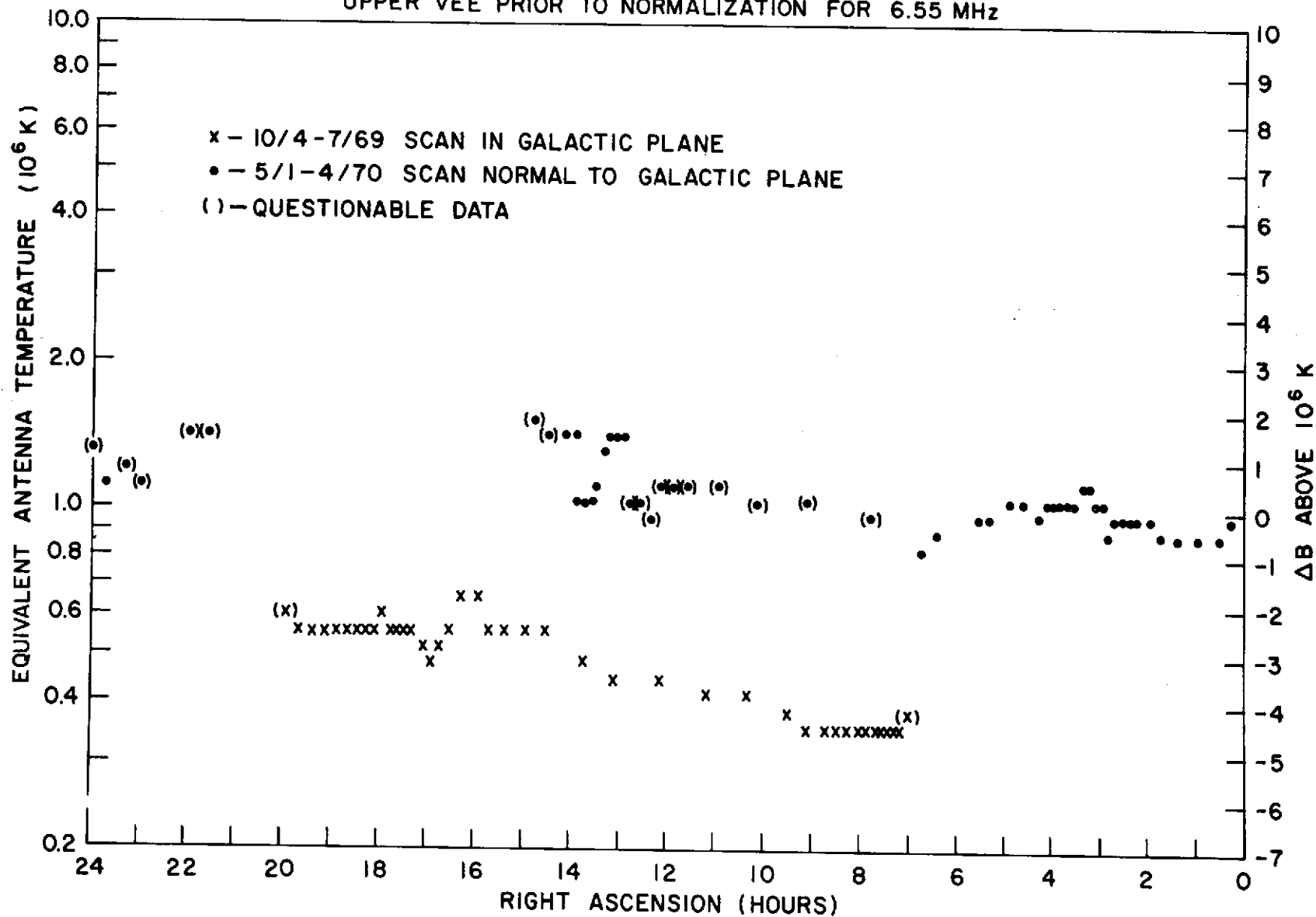
Using a large beam at 10 MHz, Clark (1967) found that the ratio of maximum to minimum brightness is about 4, and

Figure 14. - A plot of the equivalent antenna temperature (not normalized) at (a) 3.93 MHz and (b) 6.55 MHz as a function of right ascension for a scan parallel and one normal to the galactic plane indicating the low contrast visible in the original data.

COMPARISON OF THE CALIBRATED ANTENNA TEMPERATURE FOR THE
UPPER VEE PRIOR TO NORMALIZATION FOR 3.93 MHz.



COMPARISON OF THE CALIBRATED ANTENNA TEMPERATURE FOR THE
UPPER VEE PRIOR TO NORMALIZATION FOR 6.55 MHz



believes that, at 1 MHz, the brightness may be nearly isotropic. Convolving the Penticton 10 MHz (Purton, 1972) and the Parkes 30 MHz (Mathewson, et al. 1965) maps to the Vee's antenna patterns at 3.93 and 6.55 MHz also indicated that the contrast (or ratio of maximum to minimum brightness) with large beams should be less than four. Each map was convolved with the Vee antenna pattern oriented in two orthogonal directions. The smoothed maps appear in Figures 15 and 16 for 3.93 MHz and Figures 17 and 18 for 6.55 MHz for the Penticton and Parkes maps respectively.

As a check on this method of normalizing the average equivalent antenna temperature over the entire scan, the data for orbits that are normal to the initial orbits were compared to the initial data at the point where the orbits intersected. Nearly parallel orbits were not compared since these will cross at a small angle at high latitudes, and this intersection will not be well defined within the five-degree resolution of the programs. The data at the intersection points of the orthogonal orbits were examined to be sure that they were free of interference. If the data in both orbits were good, then a ratio was determined. This ratio

Figure 15. - The Penticton 10 MHz map convolved with the Vee antenna pattern at 3.93 MHz in two orthogonal orientations. Contour units are 10^4 K.

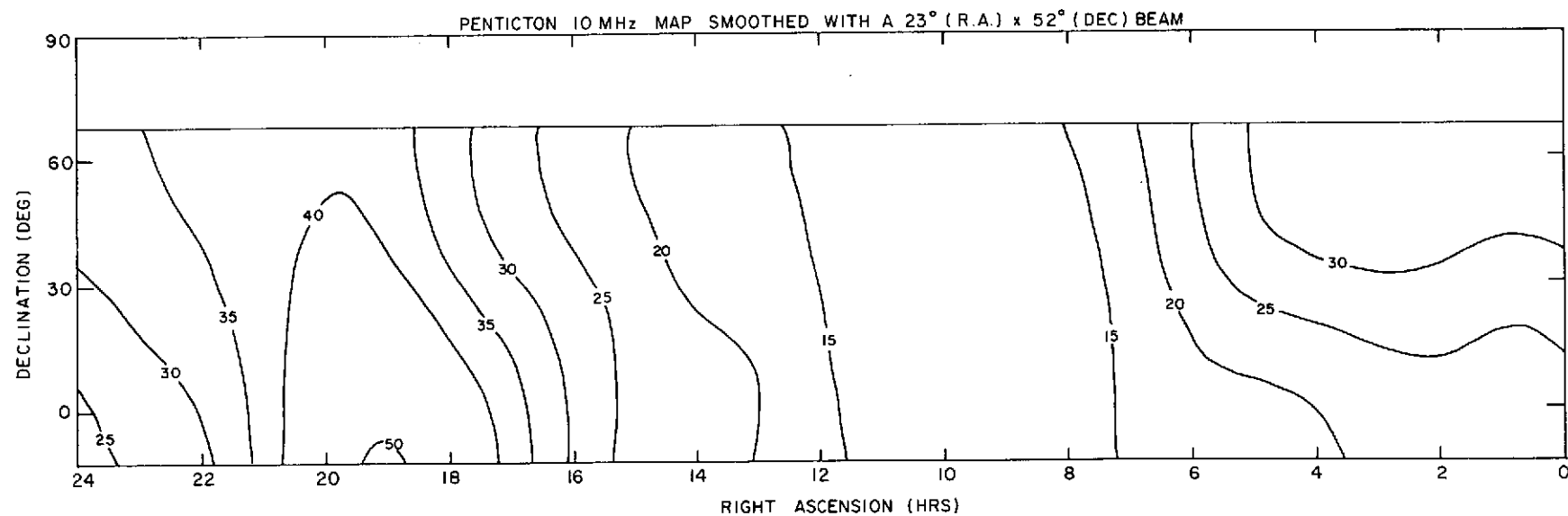
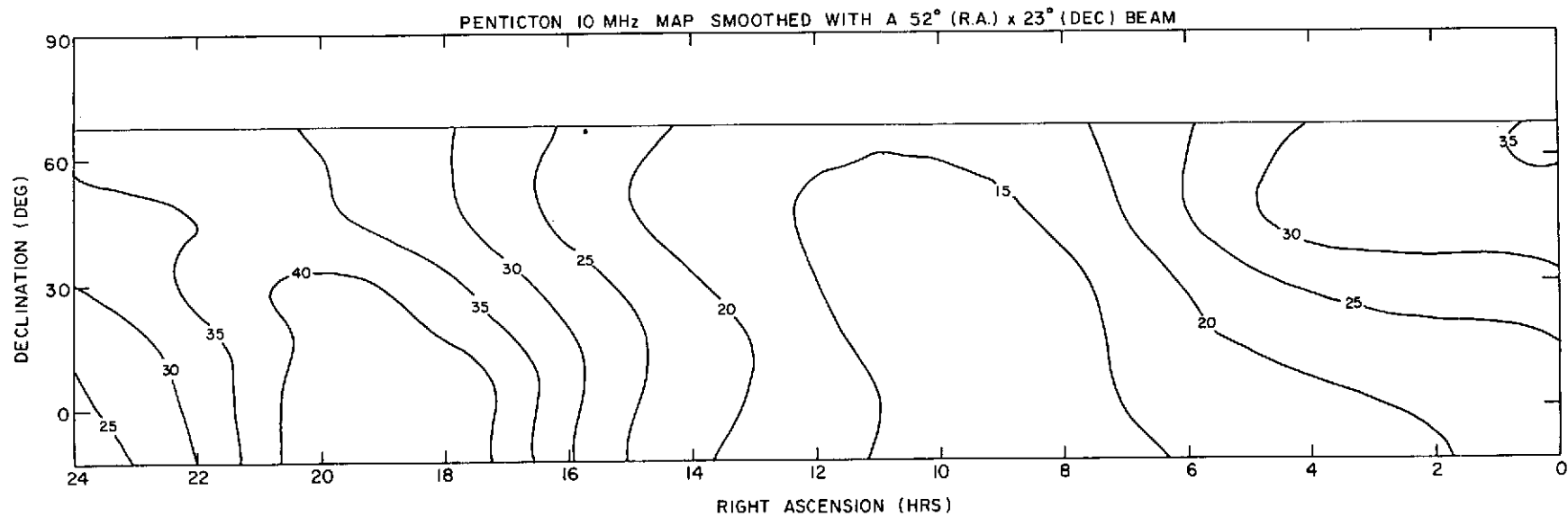
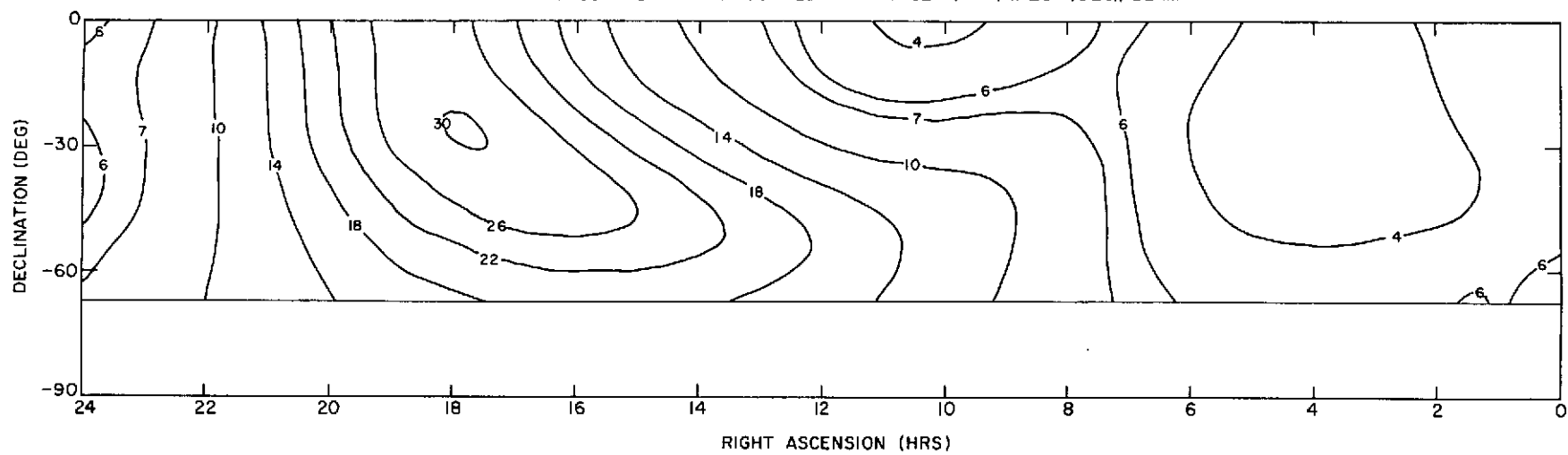


Figure 16. - The Parkes 30 MHz map convolved with the Vee antenna pattern at 3.93 MHz in two orthogonal orientations. Contour units are 1800K.

PARKES 30 MHz MAP SMOOTHED WITH A 52° (R.A.) \times 23° (DEC.) BEAM



PARKES 30 MHz MAP SMOOTHED WITH A 23° (R.A.) \times 52° (DEC.) BEAM

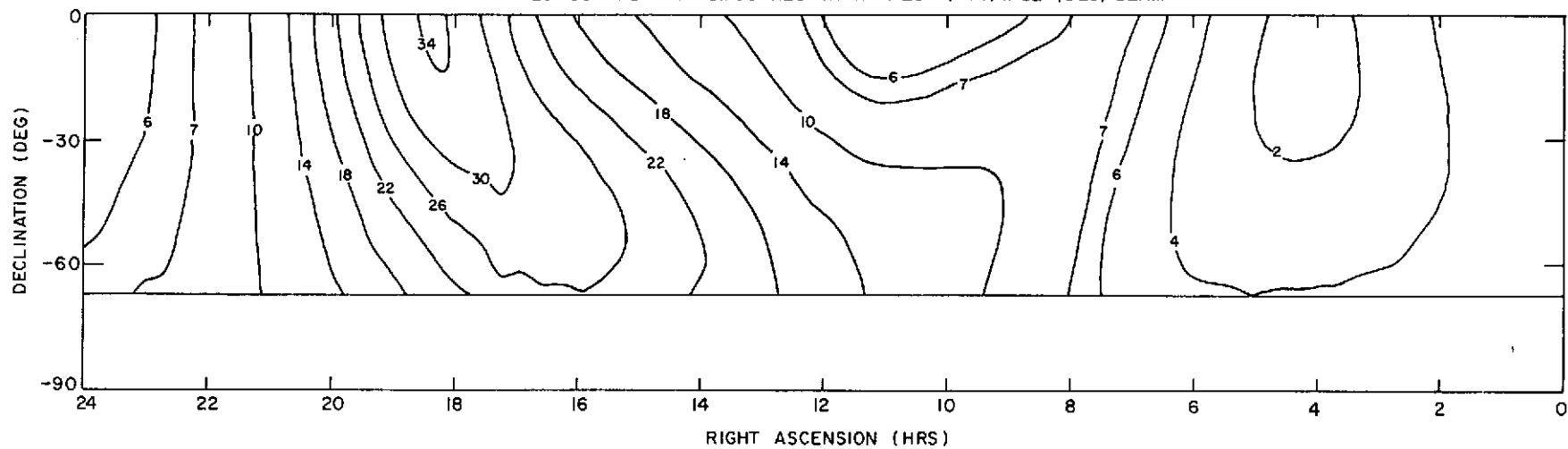


Figure 17. - The Penticton 10 MHz map convolved with the Vee antenna pattern at 6.55 MHz in two orthogonal orientations. Contour units are 10^4 K.

2-2

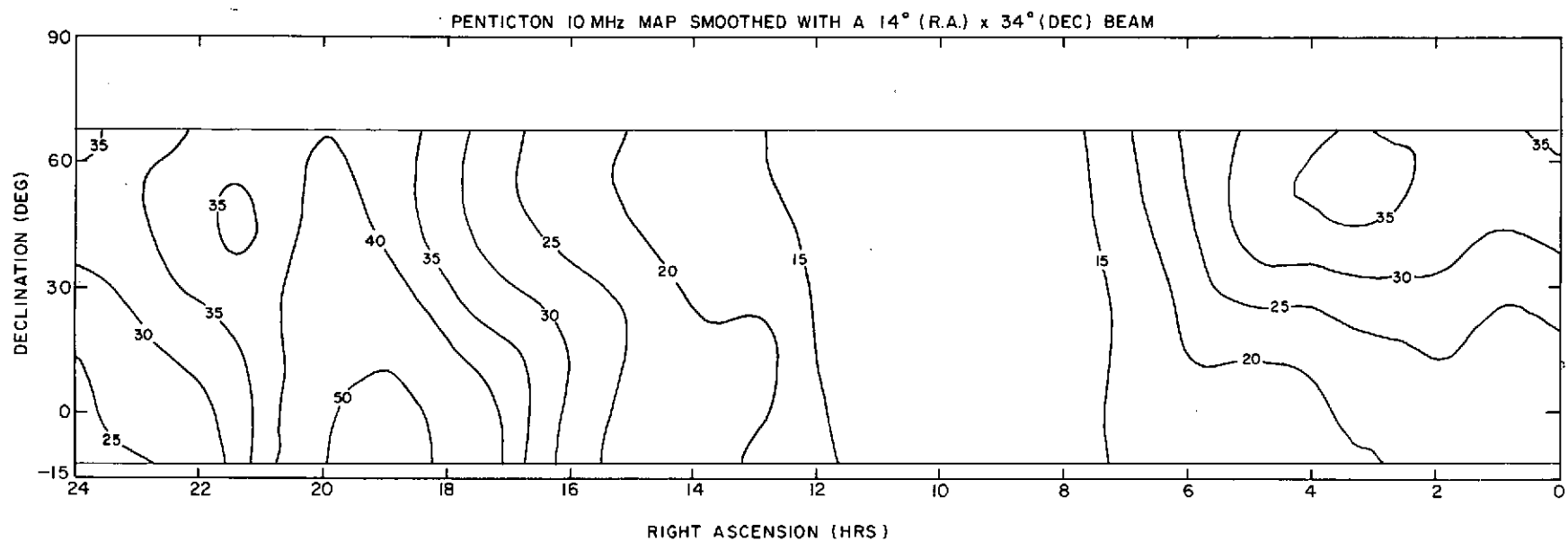
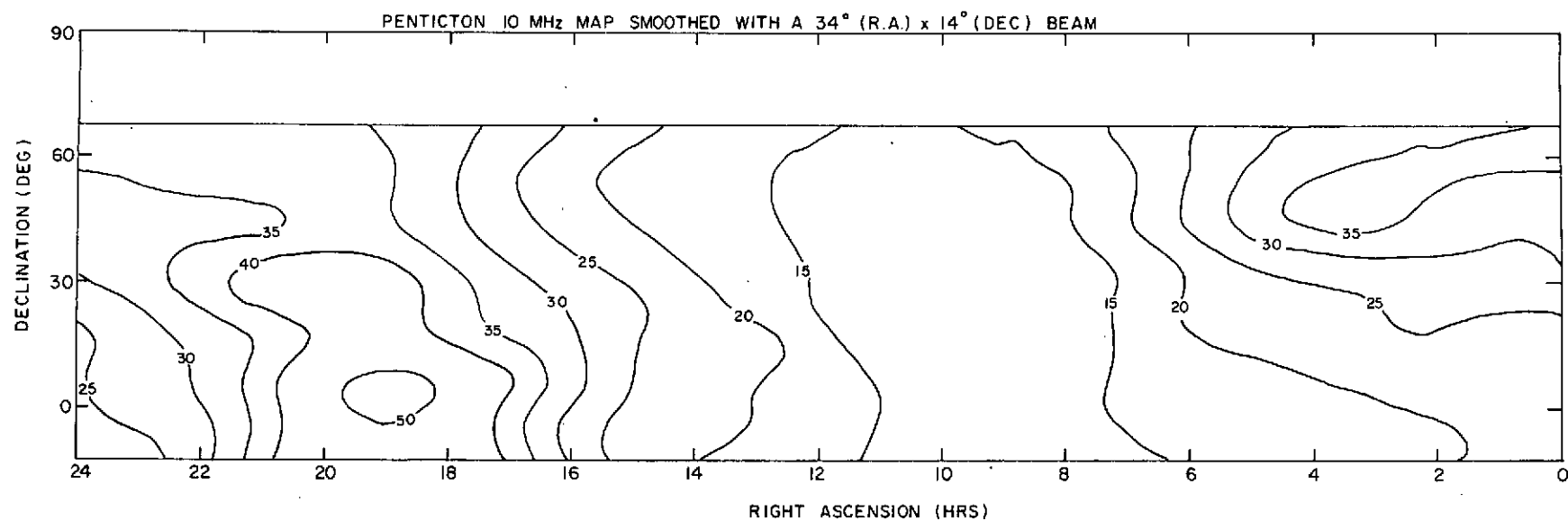
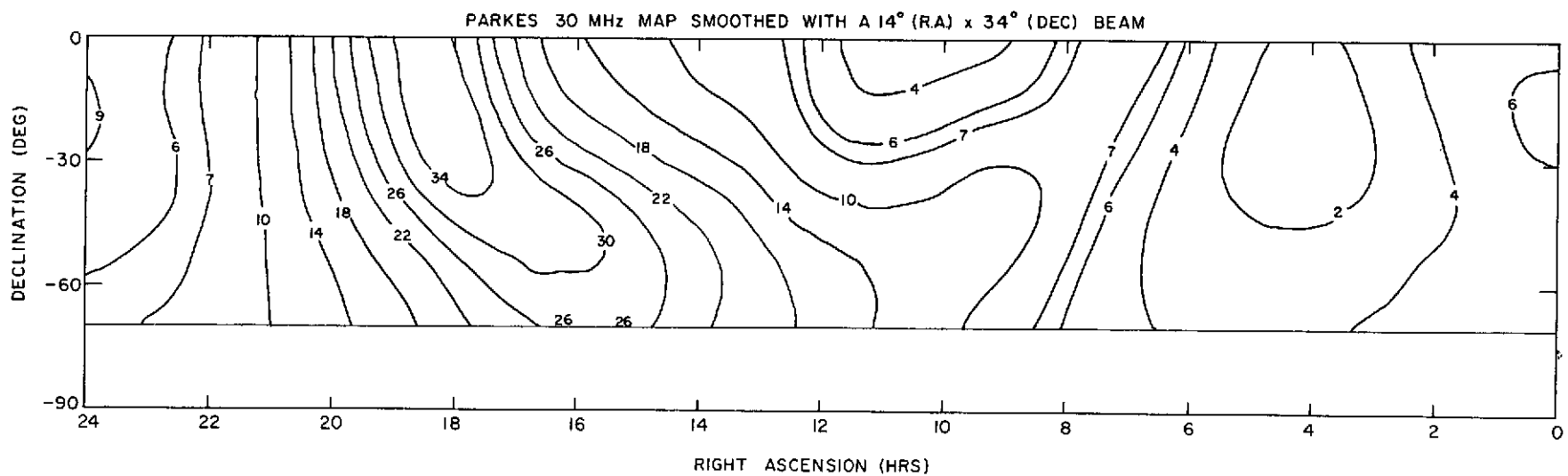
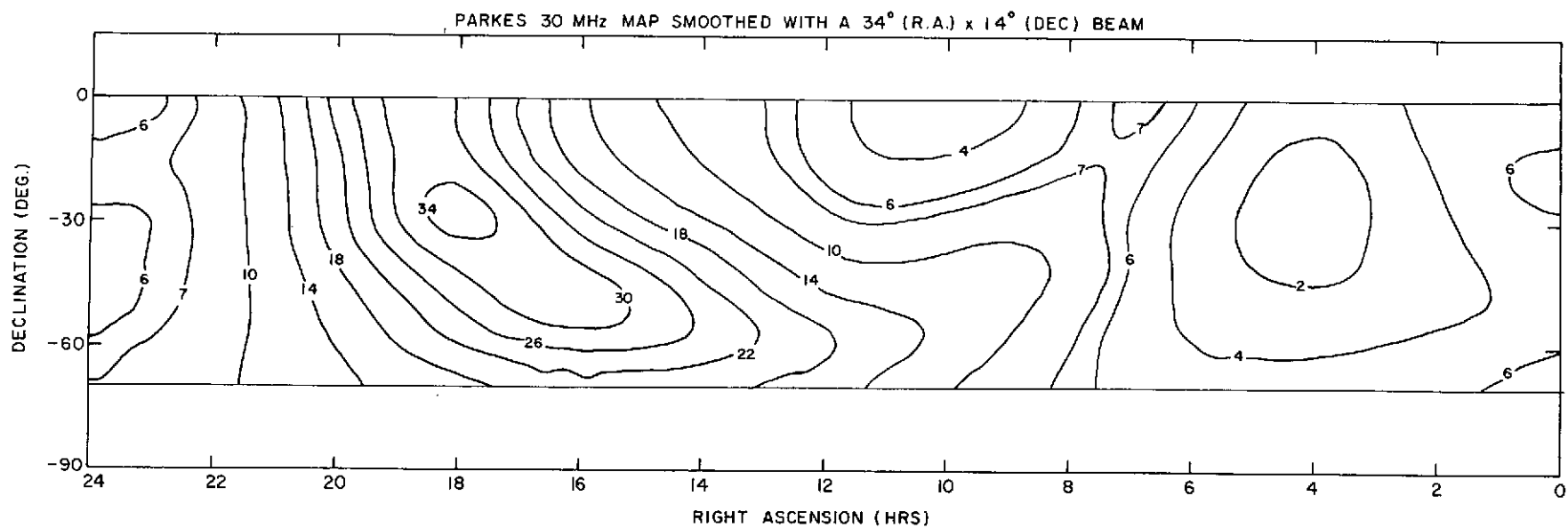


Figure 18. - The Parkes 30 MHz map convolved with the Vee antenna pattern at 6.55 MHz in two orthogonal orientations. Contour units are 1800K.



was then compared to the ratio determined by the previous method. It was found that the difference between the two ratios was usually between 5 and 7%. The digitization step for the RV receivers is 0.2 db or 5%, which would indicate that the two methods agree to well within two digitization steps which is quite reasonable. Consequently the simple minded method of correcting for receiver drift by normalizing the average equivalent antenna temperature of each four-day group to the pre-defined background level for each frequency was used to produce the maps presented in the following chapter. Antenna temperatures that have been normalized will be noted as normalized antenna temperatures to distinguish them from the equivalent antenna temperature which resulted from calibrating the observed antenna temperatures telemetered from the satellite.

V. THE MAPS FOR 3.93 AND 6.55 MHz

For each frequency, 92 files of data representing 365 days were processed through the Boxave program. The background level for each file was chosen from the histograms to represent the average galactic background. A window of ± 2 db centered on this background was used to define the range of acceptable data. The width of the window was set by an examination of the raw data. It is the narrowest window that would still include the largest expected variation of the galactic background about its average value. The minimum number of points for each five-by-five degree interval of the sky was set at 10. In any five-by-five degree interval with less than 10 points, the resulting average and standard deviation computed by the program would not reflect the galactic background, since an interval with only a few points would probably be in a region of ground breakthrough. The equivalent antenna temperatures were corrected for the receiver's instabilities by normalizing the average equivalent antenna temperature to the predefined level for each frequency. The maps of the normalized antenna temperature are shown in

Figures 19 and 20. The maps were drawn from the sky matrices by hand rather than by machine, because the machine drawn contour maps show too much detail at scale sizes well below the beam size. The erroneous fine detail originated in small-scale jitter or rapid variations of low amplitude that were superimposed over the larger-scale structure of the galactic background.

The hand drawn maps were done by color-coding the matrices, with each color representing an increment of $0.05 \times 10^6 \text{ K}$ in the range 0.6×10^6 to $1.10 \times 10^6 \text{ K}$ for 3.93 MHz and 0.25×10^6 to $0.55 \times 10^6 \text{ K}$ for 6.55 MHz. The maps shown in Figures 19 and 20 are the results of several iterations to remove apparent stripes aligned to the general orbital motion. These stripes have two characteristics that make them stand out in the maps. They are aligned preferentially along an orbit or a group of orbits and their narrow width of the order of twenty degrees. It is unlikely that the sky would be so conveniently arranged so that there would be structure in the map that aligns itself along an orbit of RAE. The origin of these structures was traced to one of three problems: (1) error in determining the average

Figure 19. - A map of the galactic background at 3.93 MHz
as observed with the RAE-1 Vee antenna.

RAE-I MAP AT 3.93 MHz FOR THE 1970 TIME PERIOD

~~~~~ EDGE OF MAP  
 - - - - - QUESTIONABLE CONTOURS  
 ——— RELIABLE CONTOURS

CONTOUR INTERVALS  
 IN UNITS OF  $10^6$  K

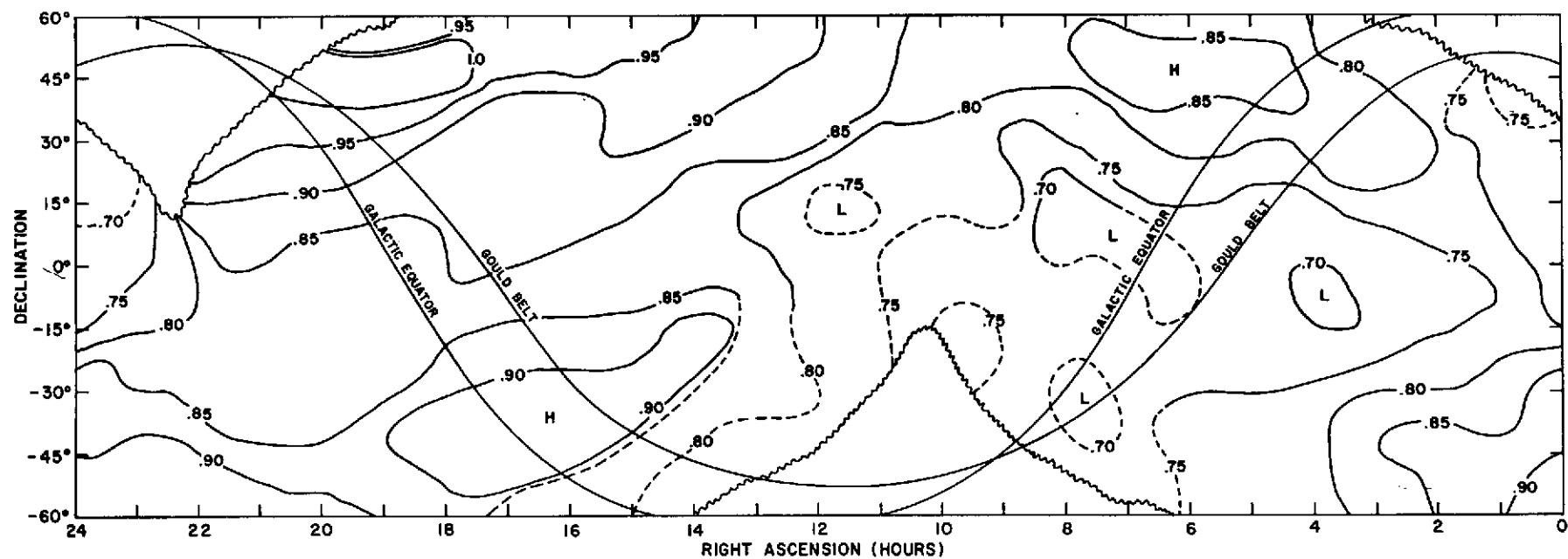
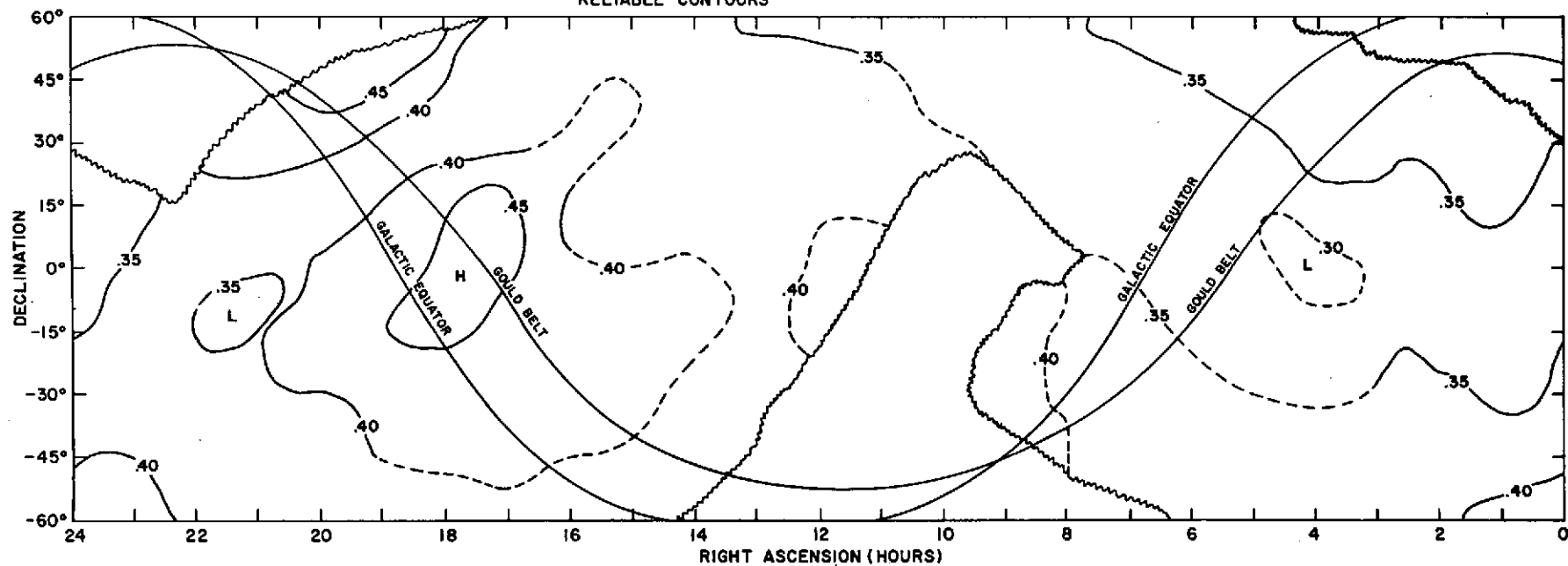


Figure 20. - A map of the galactic background at 6.55 MHz  
as observed with the RAE-1 Vee antenna

# RAE-I MAP AT 6.55 MHz FOR THE 1970 TIME PERIOD

~~~~~ EDGE OF MAP  
 - - - QUESTIONABLE CONTOURS
 ——— RELIABLE CONTOURS

CONTOUR INTERVALS
 IN UNITS OF 10^6 K



equivalent antenna temperature and hence the normalization constant for one four day group of data, (2) solar activity adding a decametric continuum for a few days, and (3) geomagnetic activity, also adding a continuum for a few days. Evidence for the solar and geomagnetic activity were obtained by examining the ESSA Research Laboratories Solar-Geophysical reports for the days in which the RV2 data were in question. Consequently these stripes were considered an artifact of the reduction process. A feature was considered a candidate for removal if it was aligned parallel to an orbit over a reasonable (such as 60°) angular extent, or if another feature in another part of the map was also aligned along the same orbit. In most cases, correcting these artifacts resulted in removal of small scale structure (small in size compared to the beam size) and in making the larger features more round in shape rather than elongated in the direction of orbital motion.

Two cross checks were performed to double check the method of normalizing the data. For four time periods (December 15-18, August 9-12, March 30, - April 2, and January 5-8, 1970), the RV1 and RV2 data were run through

Boxave separately. The two receivers should show the same response to the galactic background. In Figures 21a and b, the data (not normalized) are plotted as the difference between the weighted average of the equivalent antenna temperature and the equivalent antenna temperature for each five-degree box. The weighting of the average is by the number of points in each box and inversely by its standard deviation. To facilitate making the comparisons, the averages of RV1 and RV2 have been overlayed. The actual value of the averages for RV1 and RV2 are listed to the right of the plots. Since this data has not been normalized, the averages reflect the receiver's long term changes in gain. Keeping in mind that there are three days of data for RV2 and only one for RV1, the two sets of curves seem to reproduce each other reasonably well. The gaps in the data are caused by ground breakthrough, and the largest discrepancies are generally found in the vicinity of ground breakthrough where the data are least trustworthy.

A second check was performed by making two separate maps for the time periods January 1 - April 15, 1970 and

Figure 21. - A comparison of the equivalent antenna temperature for RV1 and RV2 at (a) 3.93 MHz and (b) 6.55 MHz for the time periods shown. The vertical scale is the weighted average of the equivalent antenna temperature minus the equivalent antenna temperature.

COMPARISON OF RECEIVER 1 & RECEIVER 2 FOR 3.93 MHz

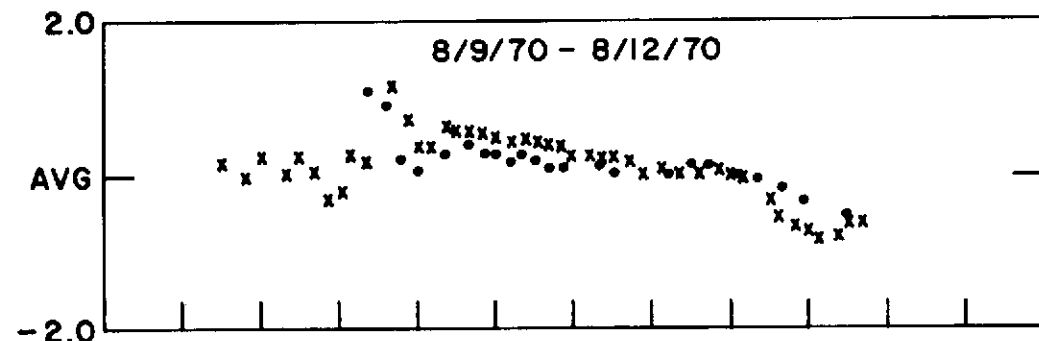
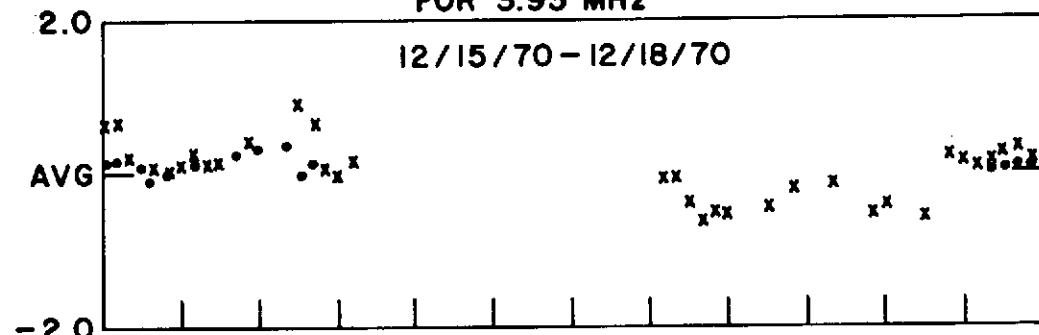
AVERAGE (10^6)
FOR



• RCVR 1 = 2.21

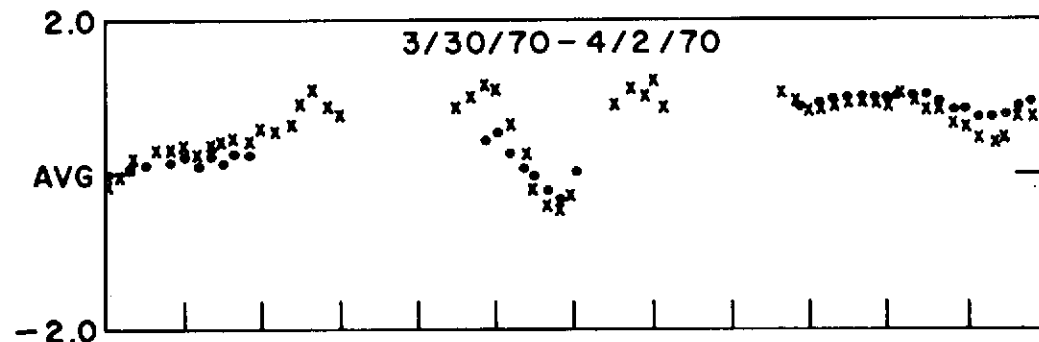
x RCVR 2 = 3.16

WEIGHTED AVERAGE MINUS THE EQUIVALENT ANTENNA TEMPERATURE $\times 10^6 K$



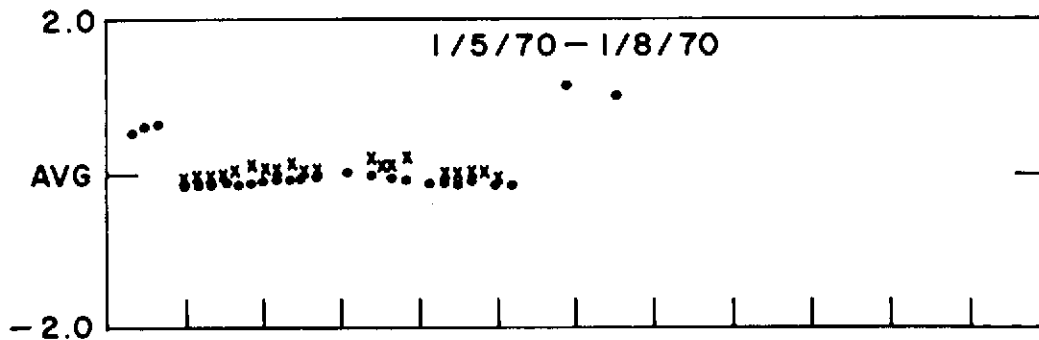
• RCVR 1 = 2.52

x RCVR 2 = 3.45



• RCVR 1 = 2.53

x RCVR 2 = 3.93



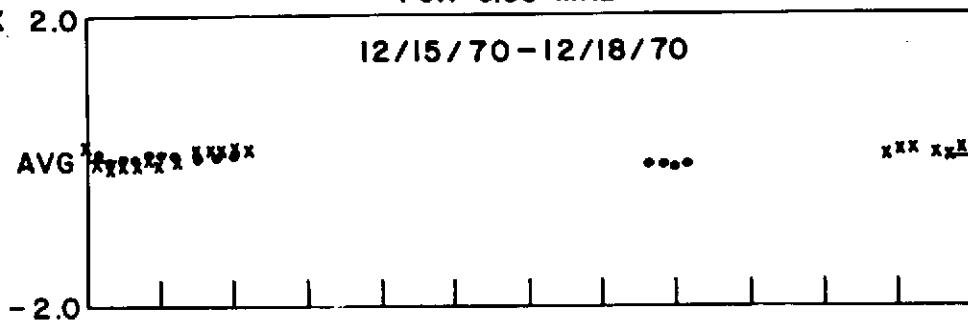
• RCVR 1 = 1.25

x RCVR 2 = 1.12

RIGHT ASCENSION (HRS)

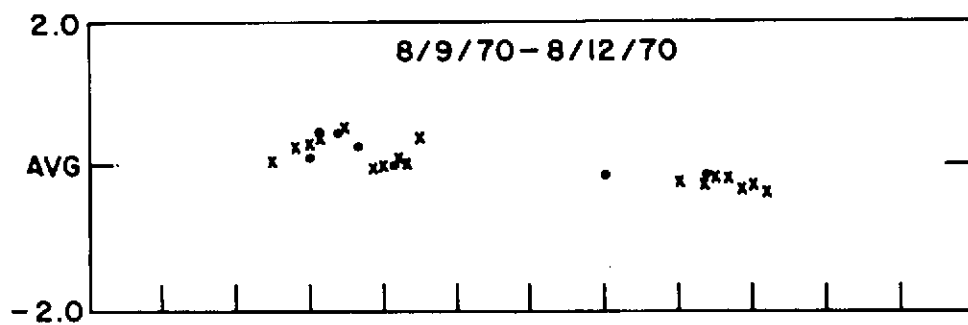
COMPARISON OF RECEIVER 1 & RECEIVER 2 FOR 6.55 MHz

$10^6 K \times$
↓

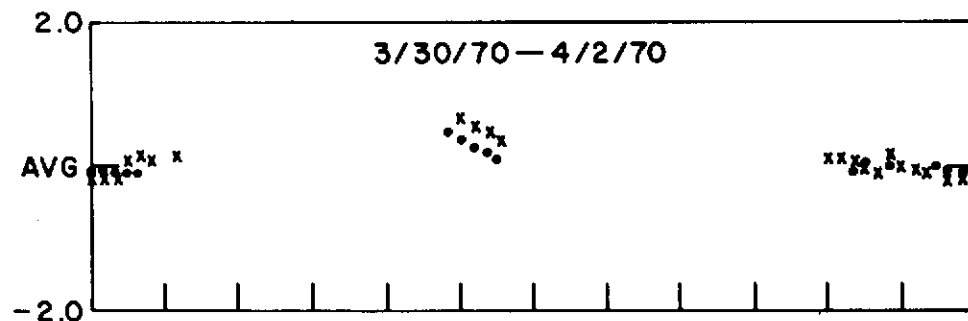


AVERAGE ($10^6 K$)
↓

• RCVR 1
x RCVR 2 = 1.03

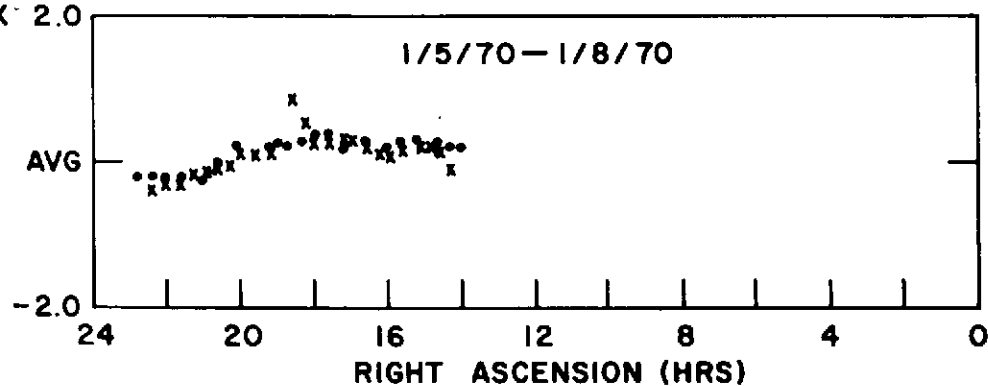


• RCVR 1 = 0.91
x RCVR 2 = 1.30



• RCVR 1 = 0.92
x RCVR 2 = 1.15

$10^5 K \times$
↓



AVERAGE ($10^5 K$)
↓

• RCVR 1 = 2.73
x RCVR 2 = 3.40

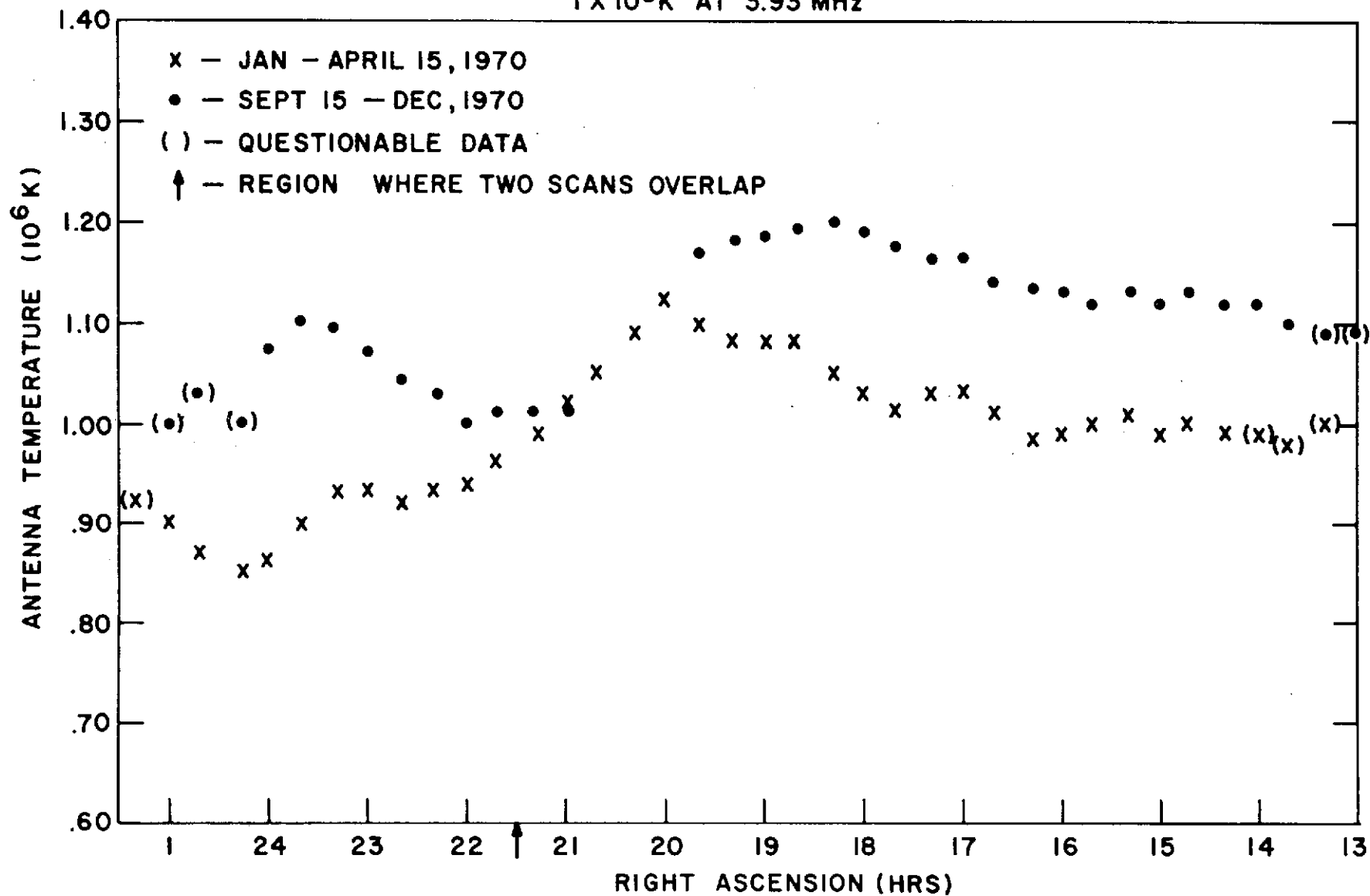
WEIGHTED AVERAGE MINUS THE EQUIVALENT ANTENNA TEMPERATURE

September 15 - December 31, 1970. These two maps are orthogonal (that is, they intersect at nearly 90 degrees) to each other. Figure 22a is a plot of the normalized (to 1×10^6 K) equivalent antenna temperature for these two scans as a function of right ascension for 3.93 MHz. Figure 22b is the same plot for 6.55 MHz. If the data reduction procedures are correct the normalized antenna temperatures should agree at the points where the two scans cross. It is unfortunate that at one of these points the data suffer from the effects of ground breakthrough. At the other point, marked by the arrow, the two temperatures do agree to better than one digitization near the point where the two orbits cross. Typical standard deviation is 7-8% where the data are good and rises to 15-20% where the data are questionable.

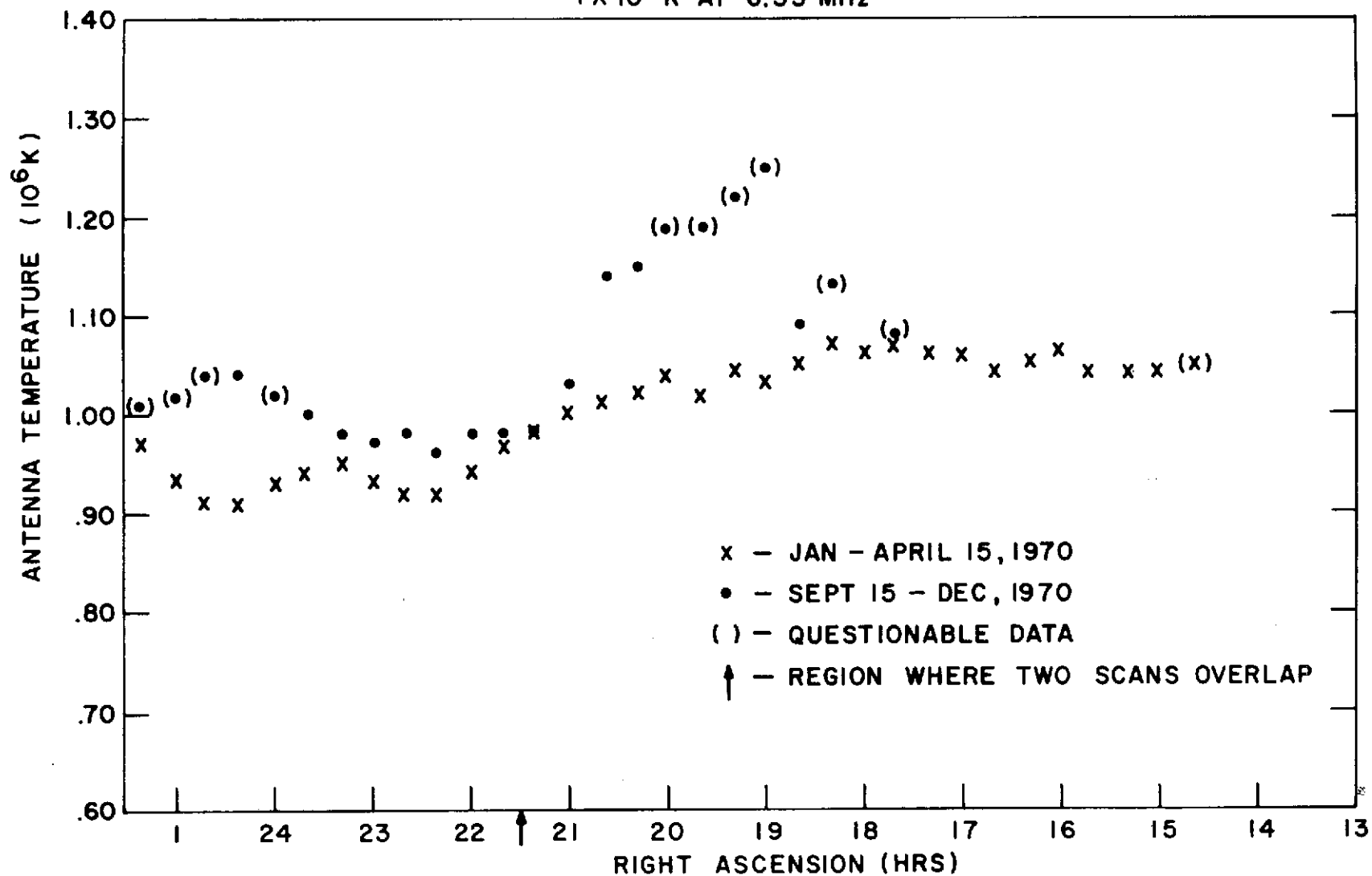
In preparing the maps, one of the main areas of concern was the possibility that some regions of ground breakthrough were not being removed completely and consequently added to the map, where they would appear as an emission feature. To provide a check against this possibility, a map of the lower Vee data was constructed using exactly the same techniques.

Figure 22. - A plot of the normalized equivalent antenna temperature at (a) 3.93 MHz and (b) 6.55 MHz for the time periods January 1 - April 15, 1970 and September 15 - December 31, 1970. The point where the scans cross is marked by an arrow. At this point the temperatures from the two time periods agree with each other indicating that the normalization period has correctly removed the receiver instability.

COMPARISON OF TWO ORTHOGONAL SCANS OF DATA NORMALIZED TO
 $1 \times 10^6 \text{ K}$ AT 3.93 MHz



COMPARISON OF TWO ORTHOGONAL SCANS OF DATA NORMALIZED TO
 $1 \times 10^6 \text{ K}$ AT 6.55 MHz



The lower Vee looks at the ionosphere which completely fills its beam. Where the ionosphere is not transparent, it reflects the galactic background much like a mirror or ground plane. Consequently the lower Vee can be considered as looking at half of the celestial sphere. The raw data (of which Figures 2 and 10 are examples) confirms this, as except for regions of ground breakthrough, there is almost no variation in the data. The map from the lower Vee should be virtually featureless, with any residual features having a scale size of about 180 degrees. Ground breakthrough, if it were being mapped, should appear as emission regions with scale sizes a good deal smaller.

As expected the map produced from the lower Vee data is quite featureless. Only the very grossest feature still exists. There is still more emission in the half of the sky centered at about 18 hours right ascension than in the other half. The contrast has been considerably reduced so that there is less than a 1 db difference between the cold and hot halves of the sky.

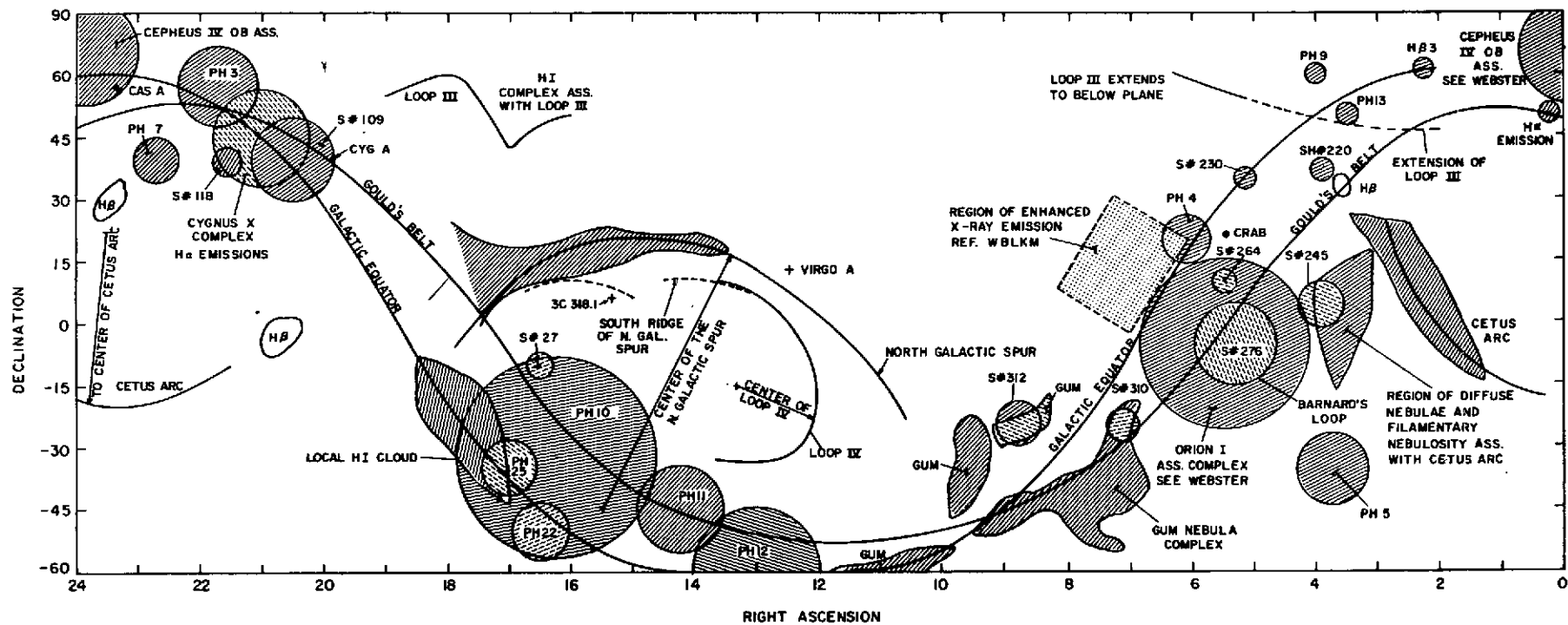
It is instructive to compare the differences in the contours of the smoothed versions of the Penticton 10 MHz

and Parkes 30 MHz maps with the Vee antenna pattern at two different orientations (Figures 14-17). The shapes of the contours undergo some relatively minor changes, but the position of the centers of the highs and lows do change. A change of position of the order of 20° can occur. This is quite consistent with the fact that the centers of the highs and lows appeared to change in the various preliminary maps made by Mr. J.K. Alexander and the author. This, then, is a measure of the positional accuracy of the RAE maps.

The smoothed maps do show the same gross features as the RAE maps, particularly a high centered roughly on the Sagittarius region and a low centered in the Orion region. The smoothed Penticton map has lost all traces of the Cygnus-X complex and nearly all traces of the North Galactic Spur. The smoothing also removed all of the discrete sources.

Figure 23 is a map of the objects that might influence a map at low frequencies. This map is intended to be a guide to help the reader correlate features found in the RAE maps (Figures 20 and 21) with known features in the sky. A one-to-one correlation should not be expected.

Figure 23. - A map of the objects one might see at low frequencies. The references are listed in Table 4.



The HII regions, if they influence the low frequency maps, will appear as regions of absorption (or alternatively low emission since only the foreground would be emitting). The PH (Prentice and ter Haar, 1969) and S (Sharpless, 1959) numbers are listed in Tables 2 and 3. The references from which the data were taken are in Table 4.

There are still some areas of the maps where the data are not as reliable as one would like. Prominent features near the boundaries of the map, such as the region centered at about 18.5 , $+55^{\circ}$ and the region along -60° declination between 19 and 24 hours should not be trusted explicitly. It is near the boundaries of the maps and at high declinations that ground breakthrough affects the data. This is the region where the statistics are relatively poor and there is more than the usual scatter in the data.

There is a bright ridge extending from 13^{h} , $+60^{\circ}$ to 15^{h} , $+30^{\circ}$ which causes the 0.90 contour to bulge out. This ridge has no corresponding feature at higher frequencies. It does align itself roughly to a group of orbits representing almost a month of data. However, the statistics are quite good (that is a large number of points with a small standard deviation in each 5 degree

TABLE 2

A list of all Stromgren spheres calculated by Prentice and ter Haar (1969, Mon. Not. R. Astr. Soc., 146, 423-444), with a radius of three degrees or larger. An asterisk denotes that it is not on the map in Figures 23.

| Object | ℓ^{II} | b^{II} | Radius
(pc) | Distance
(pc) | Angular
radius | PH
Number |
|------------------------|--------------------|-----------------|----------------|------------------|-------------------|--------------|
| III Cep | 110.3 | 3.2 | 101 | 725 | 8.0 | * 1 |
| I Ori | 206.6 | -17.6 | 212 | 460 | 26.4 | 2 |
| I Cep | 100.9 | 3.6 | 154 | 830 | 10.6 | 3 |
| II Mon | 202.9 | 2.2 | 79 | 715 | 6.3 | 4 |
| II Per | 160.7 | -16.9 | 58 | 400 | 8.3 | 5 |
| NGC2362 | 238.0 | -5.5 | 106 | 1000 | 6.0 | 6 |
| I Lac | 96.7 | -17.0 | 54 | 600 | 5.1 | 7 |
| IC2602 | 289.6 | -4.9 | 35 | 155 | 12.9 | * 8 |
| NGC1502 | 143.6 | 7.6 | 48 | 880 | 3.1 | 9 |
| II Sco | 350.6 | 18.7 | 72 | 170 | 24.3 | 10 |
| Upper Cent.
(Lupus) | 321.8 | 14.2 | 33 | 170 | 11.1 | 11 |
| Lower Cent.
(Crux) | 302.5 | 3.2 | 43 | 160 | 15.4 | 12 |
| α Persei | 148.0 | -4 | 9 | 170 | 3.0 | 13 |
| IC2391 | 270.4 | -6.9 | 10 | 150 | 3.8 | 14 |
| AO Cas | 117.6 | 11.1 | 86 | 1000 | 4.9 | *15 |
| 15 Cas | 120.8 | 0.1 | 53 | 1000 | 3.0 | *16 |
| 9 α Cam | 144.1 | 14.0 | 91 | 1000 | 5.2 | 17 |
| 24 α^2 CMa | 235.6 | -8.2 | 32 | 590 | 3.1 | 18 |
| 31 η CMa | 242.6 | -6.5 | 22 | 400 | 3.2 | 19 |
| ζ Pup | 256.0 | -4.7 | 94 | 330 | 16.3 | 20 |
| γ^2 Vel | 262.8 | -7.7 | 232 | 460 | 28.9 | 21 |
| HD150136 | 336.7 | -1.6 | 78 | 700 | 6.4 | 22 |
| μ Nor | 339.4 | 2.5 | 85 | 1000 | 4.9 | 23 |
| HD149404 | 340.5 | 3.0 | 86 | 800 | 6.2 | 24 |
| HD154090 | 350.8 | 43 | 48 | 480 | 5.7 | 25 |
| ζ Oph | 6.3 | 23.6 | 54 | 170 | 18.2 | 26 |
| HD193322 | 38.1 | 2.8 | 72 | 650 | 6.3 | 27 |
| 68 A Cyg | 87.6 | -3.9 | 72 | 750 | 5.5 | 28 |
| 26 Cep | 108.5 | 6.4 | 56 | 830 | 3.9 | *29 |

TABLE 3

List of HII regions with a diameter 5° or greater.

Data taken from Sharpless (1959, Ap. J. Suppl. #4, p. 257).

| RA(1900) | Dec | Diameter
degrees | Sharpless
number | Comment |
|------------------------------------|----------------------------------|---------------------|---------------------|---|
| 16 ^h 31. ^m 7 | -10 ^o 22 ¹ | 8.0 | 27 | ζ Oph is the exciter |
| 20 30.0 | 40 00 | 18.0 | 109 | Cygnus Nebula |
| 21 33.0 | 39 46 | 8.0 | 118 | |
| 3 54.1 | 36 20 | 5.3 | 220 | |
| 5 15.9 | 34 02 | 5.0 | 230 | May be part of I Aur ass. |
| 3 57.3 | 3 51 | 12.0 | 245 | |
| 5 29.7 | 9 52 | 6.5 | 264 | λ Ori is exciter |
| 5 22.5 | -4 03 | 20.0 | 276 | The Barnard Loop |
| 7 08.9 | -24 25 | 8.0 | 310 | Incomplete ring,
contains cluster
NGC 2362 |
| 8 54.8 | -25 18 | 12.0 | 312 | Size uncertain because
of southern limit of
Palomar Atlas |

TABLE 4

REFERENCES FOR FIGURE 23

Gould's Belt: Gum, Collin S. Memoirs, R.A.S. 67, (1954).

Galactic Spurs & Loops Defined by Max Radio Brightness:

Haslam, Kahn, and Meaburn Astron. & Astrophys. 12, 388 (1971).

HB3 - Roger, R.S., Ap. J. 155, 831 and Bridle, A.H. Mon. Not.

R. Astr. Soc. 138, 251-258.

Width of Cetus Arc: Meaburn, J., Z. Astrophys. 65, 93 (1967).

Width of North Galactic Spur: Holden, D.J. Mon. Not. R.

Astr. Soc. 145, 67, (1969).

WBCKM Williamson, Bunner, Coleman, Kraushaar, McCammon: AAS

Meetings, E. Lansing, Mich. August 1972.

Local HI Cloud: Riegel and Crutcher Astron. & Astrophys.

18, 55 (1972).

CAS A, CYG A, VIRGO A, CRAB: Kraus, J.D. Radio Astronomy,

McGraw-Hill, 1966.

Cygnus X Complex, H α at 0^h20^m, 50^o from Courtes & Sivan,

Astrophysical Letters 11, 159 (1972).

Gum Nebula Complex: Alexander, J.K. (1971), The Gum Nebula

and Related Problems, NASA X-683-71-375.

S#'s: HII Regions from Sharpless, Stewart (1959) Ap. J.

Suppl. #4, p. 257, see Table 3.

TABLE 4 CONTINUED

Orion I and Cepheus IV Associations, Webster, W.J., Jr.,

(1971) The Gum Nebula and Related Problems, NASA

X-683-71-375.

PH#'s: Stromgren Spheres from Prentice, A.J.R., and Ter

Haar, D., (1969) Mon. Not. R. Astr. Soc., 146, 423.

See Table 2.

H β Emission Regions: Johnson, H.M. (1972), Ap. J. 174,

591.

box) which would indicate that this ridge is a real feature. But because of its high declination and its alignment with a group of orbits, it should not be trusted explicitly.

The RAE maps at 3.93 and 6.55 MHz (Figures 19 and 20 respectively) are quite similar in their overall appearance. They basically show a cold part of the sky, centered in Orion, and a hot part centered in Sagittarius. Neither the galactic plane nor the Gould Belt are very obvious.

The galactic spurs and loops, such as the North Galactic Spur and the Cetus Arc, are believed to be relatively nearby structures, primarily because of their large angular size. They are prominent features at higher frequencies. They show evidence of magnetic field structure and regions of filamentary nebulosity. It has been suggested that they are possibly very old supernova remnants (Haslam, et al, 1971). If they are nearby supernova remnants, and if their spectra do not turn over above RAE's observing frequency, they could be prominent features in the RAE maps. The loops would be visible as

ridges of emission. If the loops do represent the edges of very extended supernova remnants, it may be possible, at low frequencies, to see emission from the entire remnant. If this was the case, it would appear as a region of emission with the loop more or less lying along its edge. Similarly the filamentary nebulosity associated with some of them would appear as regions of absorption if they were large enough and had a sufficiently high average thermal electron density.

There is a prominent bright region at about $18^{\text{h}}.5$, $+55^{\circ}$ that is just inside Loop III that may be related to it. However, because this region is at the edge of the map and in a part of the sky where the data are subject to ground breakthrough, this association cannot be taken as certain. Similarly regions near the boundaries of the map, such as the region along -60° declination from 19 to 24 hours, should not be trusted explicitly.

The Cetus Arc may be present in the map. At $23^{\text{h}}.5$, $+15^{\circ}$ there is a region of low emission that is near the center of the Arc. And at 2^{h} , $+15^{\circ}$, where the Arc is most prominent at higher frequencies, there is a ridge of

slightly higher emission. There is also some weak evidence of Loop III, in that there is a bright region at 6^{h} , $+50^{\circ}$ that is just inside the Loop.

There is a ridge of emission at 3.93 MHz from 18^{h} , $+10^{\circ}$ to 14^{h} , $+20^{\circ}$ which causes the 0.85 contour to bulge out. It appears to correspond to the main part of the North Galactic Spur. In the original map, the ridge is somewhat separated from the gradient at higher declinations. The ridge can also be seen continuing along the center of the Spur, however, the amplitude of the ridge is less than one standard deviation. The gradient that appears in this part of the sky is then a blend of three features; an actual gradient running from 22^{h} to 14^{h} at declinations above $+15^{\circ}$, the ridge possibly associated with the North Galactic Spur and a ridge mentioned previously, at 18.5^{h} , $+55^{\circ}$ that has no obvious association with a feature at higher frequencies.

At 6.55 MHz, there is a high centered near the base of the North Galactic Spur. Again in the original map, there is a ridge extending along the arc of the spur, but the amplitude of the ridge is less than one standard deviation.

If the Spur is a supernova remnant that exploded out of the galactic plane, it would appear reasonable to assume that emission associated with its leading edge would be concentrated where the edge meets the galactic plane, as this would be the place where there would be more material to be compressed. It would give a more extended region of emission at these lower frequencies. Add to this, the possibility that at low frequencies it might be possible to see all of its shell and not just the places where the shell is seen edge on, and the result may be a region of emission that is not exactly centered on the area of the sky encompassed by the North Galactic Spur.

The large bright region at $16^{\text{h}}.5, -35^{\circ}$ is centered approximately on the II Sco Association. However, if this association has a Stromgren sphere as large as that calculated by Prentice and ter Haar (1969), then it should appear as a region of absorption. Because it is bright this would indicate that either there is a region of low frequency synchrotron emission in front of the association or that there is no significant HII region associated with

the II Sco Association and that the emission is coming from beyond it and more than likely from the Sagittarius arm. At 6.55 MHz, this feature is blended with the feature attributed to the North Galactic Spur. The data at 6.55 MHz for this part of the sky is particularly plagued with ground breakthrough.

The Orion complex does appear as a region of absorption. However, the region extends further north of the galactic plane than the optical HII region. This entire complex has a lot of HII regions with low emission measure, which would still appear in absorption at low frequencies. There is a study of faint H β and H α emission being conducted at Goddard (Reynolds, et al. 1972) but their data for this part of the sky are not yet reduced. Near the edge of the maps, at $7.6^{\text{h}}, -40^{\circ}$, is some evidence that the Gum Nebula is present in absorption; however, the statistics for the data in this part of the sky are not good.

There are parts of the maps that still have problems chiefly because of ground breakthrough. By adding data from other time periods, it is possible to remove most, but not all, problems. This is because the occurrence of

ground breakthrough over one part of the world does have some seasonal variability. By adding data from other time periods, there is the possibility of scanning a part of the sky without having ground breakthrough. In addition by adding more data, one can improve the statistics for data in those areas where ground breakthrough always presents a problem. Complicating the issue, of course, is the problem of correctly normalizing the additional maps. This work has begun and the first preliminary maps are shown in Figures 24 and 25. The maps were made by averaging the 1970 map with the late 1968 - early 1969 and 1971 maps. The averaging was weighted by the number of points and inversely by the standard deviation of the individual elements in the three maps. Note that the combined maps are normalized to 1.0×10^6 K for both 3.93 and 6.55 MHz and not to 0.89×10^6 and 0.38×10^6 K for the 1970 maps. Additional work in combining all of the data is in progress at the time of this writing. The contours plotted are at 1/3 db intervals. The galactic plane (and/or the Gould Belt since with this resolution they are the same) is more noticeable than in

Figure 24. - The first preliminary map of the galactic background at 3.93 MHz as observed by the RAE-1 Vee antenna using all of the available data. The map is normalized to 1.0×10^6 K.

3.93 MHz MAP USING ALL OF THE 1968-1972 DATA NORMALIZED TO 1×10^6 °K

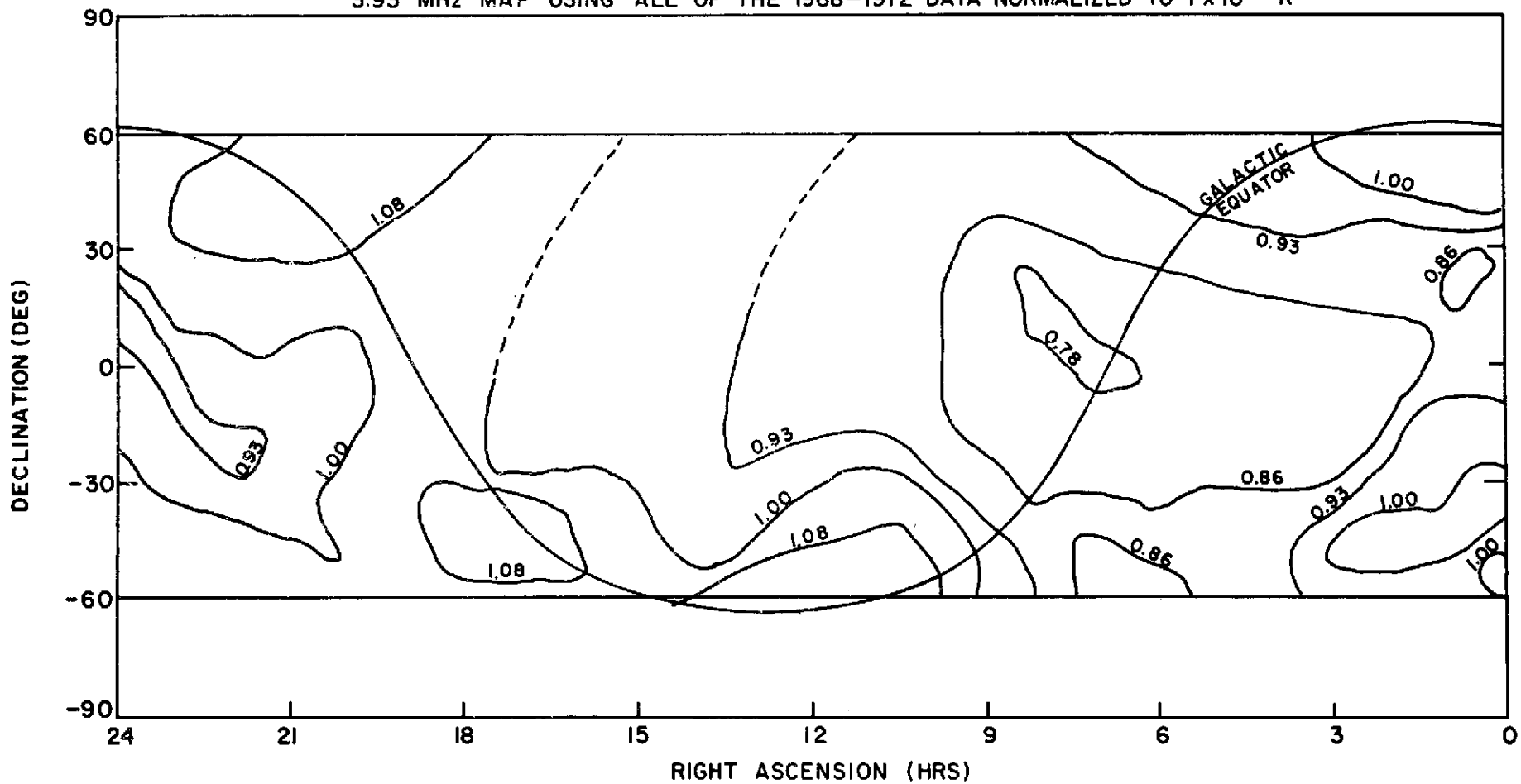
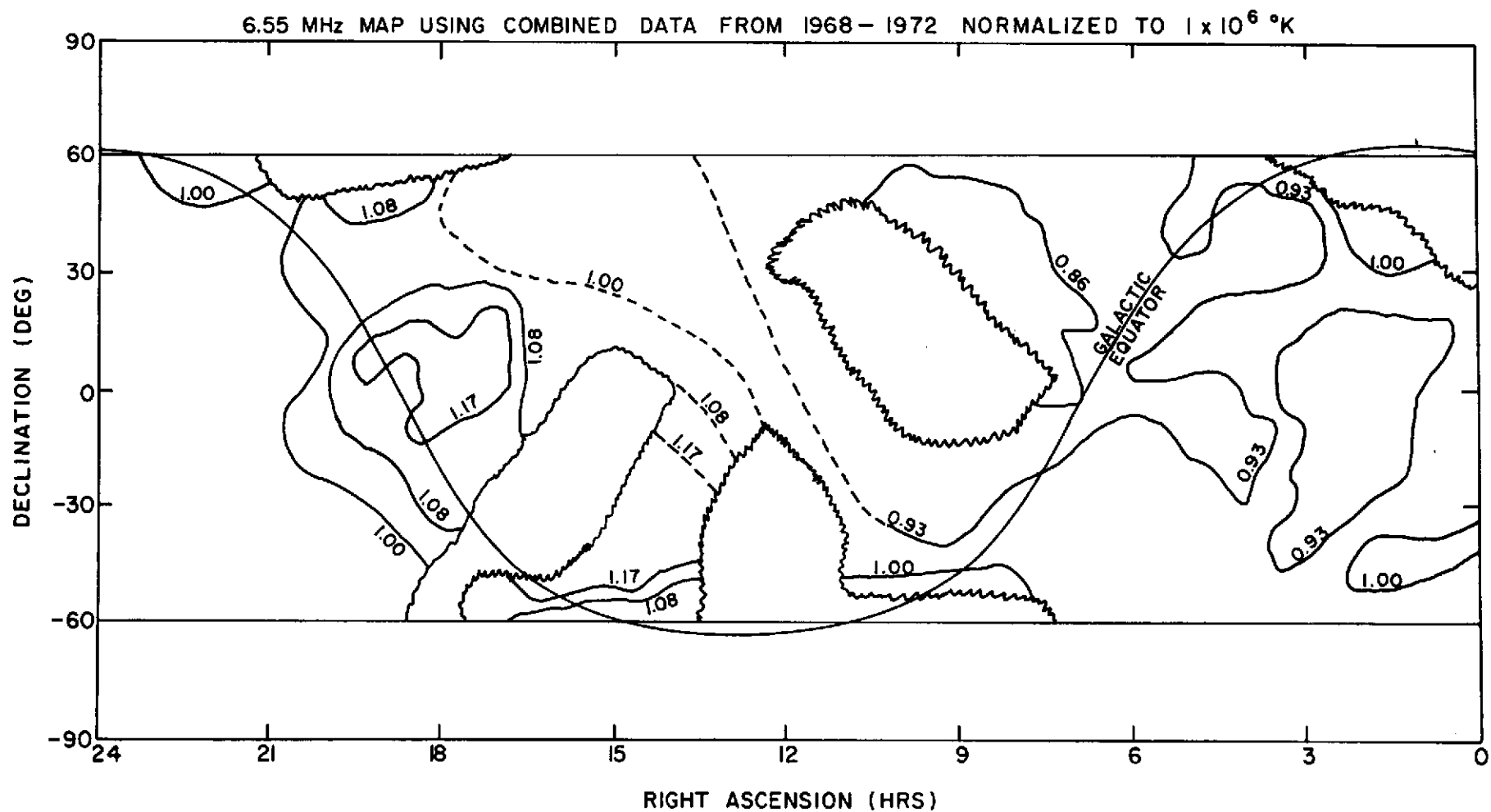


Figure 25. - The first preliminary map of the sky at 6.55 MHz as observed by the RAE-1 Vee antenna using all of the available data. The map is normalized to 1.0×10^6 K.



the 1970 maps. The Cetus Arc and the Gum Nebula are no longer as apparent. At 3.93 MHz, the North Galactic Spur has also disappeared, but at 6.55 MHz, the base of the Spur is still visible.

VI. SUMMARY

The objective of this thesis has been to produce a map of the galactic background from the RAE data for two frequencies -3.93 and 6.55 MHz. The first three chapters supply the reader with the necessary background. They contain a brief overview of the field of low frequency galactic radio astronomy, a description of the satellite and its hardware, and a description of the data processing system.

The data from the upper Vee antenna are discussed in Chapter IV. The chapter's main emphasis is the problems encountered in processing the data (in particular receiver instability and ground breakthrough) and the methods used to eliminate or minimize their influence on the maps.

Ground breakthrough can be filtered out by restricting the range of antenna temperatures permitted to pass through the filter. As a demonstration that ground breakthrough is not incorporated into the maps, a map from the data from the lower Vee was constructed. As expected, this map was virtually featureless with no discrete emission

regions (which would have been evidence for ground breakthrough appearing in the map). Ground breakthrough does affect the data in that the statistics for the data in the regions of the map with ground breakthrough are considerably poorer than regions that are not affected by ground breakthrough. Not only is the standard deviation of the data considerably larger when ground breakthrough is present, but the total number of data points is considerably reduced. This then lowers the overall reliability of those portions of the map that suffer from ground breakthrough.

The receiver instability problem was removed by normalizing the average of the galactic background for each four day group of data to a defined background level. This defined background level was determined from the averages of the galactic background for the first ten months of operations when the receiver was known to be stable. The justification for using this technique was based on the low contrast exhibited by the raw data from the upper Vee antenna and from the Penticton 10 MHz and Parkes 30 MHz maps after smoothing with a antenna beam pattern similar to the Vee antenna.

In Chapter V, the construction of the map for 3.93 and 6.55 MHz is discussed. They are compared with the two smoothed versions of the Penticton and Parkes maps with the Vee antenna pattern in two orthogonal orientations. It is shown that the positional accuracy of the RAE maps is about 20° . While the RAE maps have an overall similarity with the smoothed Penticton and Parkes maps, they contain some different features. At 3.93, and to a lesser extent 6.55 MHz, one's "view" is limited by the opacity of the interstellar medium, particularly in the galactic plane. It is quite likely that the differences between the RAE maps and the smoothed Penticton and Parkes maps are a reflection of the large scale structure of the interstellar medium in the local part of the Galaxy.

It is unfortunate that the project's goal of mapping "the background with at least an order of magnitude better resolution than is provided by a dipole antenna" [page 5] was only partially attained in that the actual resolution in the maps is about a factor of two lower than what had been desired. The resolution has been degraded due to a twofold effect, that of the large side lobes along the

minor axis of the antenna beam, which has the effect of lowering the contrast, and the necessity of combining orthogonal scans in order to counteract the influence of ground breakthrough. Very recently the Radio Astronomy Branch has received a preliminary study of the behavior of the RAE antenna booms over its lifetime by AVCO of Wilmington, Mass. This study indicates that because of the gravity gradient forces on the antenna booms, the closure angle of the Vee antenna is not 50° as expected, but more like 35° . The most significant effect is that the main beam at 3.93 MHz is larger, on the order of 40° in the E plane (the plane of the booms). The main beam in the H plane is also enlarged, but not nearly as much. The result is that the main beam is now more nearly circular at about 40° than previously believed. This would be consistent with the reduced angular resolution in the maps presented in this study.

THE APPENDIX

The RAE-B Satellite

In all projects of this nature, one set of conclusions can be placed in the "if I had to do it over again" category. RAE-B is this second chance, and in this Appendix I will outline the changes made in the RAE mapping experiment with the Vee antenna to accommodate the lessons learned from RAE-1.

RAE-B is the second satellite of the Radio Astronomy Explorer series and is currently scheduled for launch in mid-June of 1973. Its operation will be different from RAE-1 in that it will be placed in orbit around the moon. Placing the satellite in lunar orbit has several advantages. Among the most noticeable will be the reduction in the interference from the earth's ionosphere and ground breakthrough. This interference will be reduced by a factor of roughly 44 db by going to lunar orbit. However, since ground breakthrough has been consistently measured at 40 db (where the receivers saturate) above the galactic background, going to lunar orbit will not eliminate it completely.

Furthermore, the earth as seen from lunar orbit will subtend only a small fraction of the antenna beam so the portion of the satellite's orbit that will be affected is quite small and on the order of the size of the antenna beam. The earth noise now has one useful aspect, for the earth will look somewhat like a point source and accordingly the antenna pattern will be mappable without resorting to mathematical or scale models.

The moon will not completely fill the lower Vee antenna pattern at 3.93 MHz and below. This will allow occultation measurements of likely small sources of low frequency emission such as Jupiter.

The prime disadvantage of a lunar orbit is the very slow precession rate of $0.14^\circ/\text{day}$. This means that the satellite will take nearly four years to map the sky, and hence only one map will be produced if the satellite will last as long as RAE-1. Offsetting this disadvantage slightly will be the increase in the integration time for each part of the sky.

The satellite has had several modifications to improve its performance over that of RAE-1. The tape recorder has

been improved since it will be quite important in this mission. When the satellite is behind the moon, the moon will shield the satellite from earth noise and make measurements of the galactic background a good deal easier. However without the tape recorder this will be useless since the satellite is also out of communication with the earth at that time.

The thermistor bridge power meters have been redesigned to incorporate solid state switches in place of the reed relays that failed on RAE-1. This will greatly improve the lifetime of these instruments. Since they are temperature insensitive, the "fine" telemetry channel will avoid the temperature sensitive problems that have occurred on RAE-1.

Finally each Vee antenna will have one Ryle-Vonberg receiver and one burst receiver. (The burst receivers are simple total power receivers with a rapid time response.) The burst receivers are internally calibrated to allow for correction of receiver drift. A careful inter-comparison between the RV and burst receiver's responses to the galactic background and the burst receiver's calibrator will allow

for removal of any temperature effects or long-term receiver drift that does occur. One of the new computer programs that will be developed will monitor the relative performance of the two receivers and keep a detailed history that will provide for removal of these long-term effects.

The pre-launch calibration procedures have been improved. The most significant change is that each receiver will be calibrated at five, not three, environmental temperatures that span the temperature range that the satellite is expected to operate. This will allow a five point interpolation rather than the three point interpolation that is now done on RAE-1. Also on RAE-1 the calibration data were fitted with fifth order polynomials. The resultant curves were then used to calibrate the telemetry data. On RAE-B, the five adjacent calibration points nearest the telemetry data will be used to perform an interpolation to calibrate the telemetry data. The fifth order interpolation will fit the data to well within the telemetry errors and has been demonstrated to work successfully on IMP-6.

The Vee antennae are carbon copies of each other. In the event of a complete failure of the upper Vee, the satellite may be inverted and the impact on the galactic mapping program minimized.

In spite of the small precession rate and consequently the small scanning rate of the celestial sphere, the prospect of RAE-B providing good quality maps of the galactic background with some angular resolution at frequencies well below the normal ionosphere cut off are very bright indeed. There is a real possibility that with RAE-B it will be possible to do a map not only of antenna temperature but of spectral index between a pair of frequencies.

REFERENCES CITED

- Alexander, J.K., Brown, L.W., Clark, T.A. and Stone, R.G., 1970, Astron. and Astrophys., 6, 476.
- Andrew, B.H., 1969, Mon. Not. R. Astr. Soc., 143, 17-25.
- Blanchard, D.L., 1969, Dynamical Performance to Date of RAE-A (Explorer 38), NASA Document X-723-69-214.
- Brown, L.W., 1973a, Ap. J., 180, 359.
- _____, 1973b Winter URSI Meeting
- Cariga, L., 1971, "Radio Astronomy Explorer (RAE) Satellite Analog-to-Digital (A/D) Conversion", NASA Contract NAS 5-11790.
- Clark, T.A., 1967, Ph.D. Thesis, University of Colorado.
- Clark, T.A., Brown, L.W. and Alexander, J.K., 1970, Nature, 228, 648.
- Collins Radio Company, 1966, "Experimental Studies of Current Distributions and Radiation Patterns of a Resistively Loaded V-antenna at Quarter Scale for a Radio Astronomy Explorer Satellite", NASA Contract No. 5-9255.
- Duff, B.M., 1964, Harvard University Science Report, Nsb-579-3.
- Ellis, G.R.A. and Hamilton, P.A., 1966, Ap. J., 143, 227-235.
- Ferris, A.G. and Shea, J.T., 1968, NASA-GSFC Operations Plan 9-68 Radio Astronomy Explorer RAE-A, NASA Document X-513-68-183.
- Field, G.B., Goldsmith, D.W., Habing, H.J., 1969, Ap. J. Letters, 158, L73.
- Hartz, T.R., 1964, Ann d'Astrophys, 27, 823.
- Herman, J.R. and Caruso, J.A., 1972, "Radio Astronomy Explorer (RAE-1) Observations of Terrestrial Radio Noise", NASA Contract NAS 5-11385, submitted to Planetary and Space Sciences.

Hjellming, R.M., Gordon, C.P., Gordon, K.J., 1969, Astron. and Astrophys., 2, 202.

Iizuka, K., 1965, Harvard University Science Report, Nsb-579-4.

_____. , 1967, IEE Trans. Ant. & Prop. Ap.-15, 236.

Kaiser, M., 1972, Private communication.

Machin, K.E., Ryle, M. and Vonberg, D.D., 1952, Proc. IEE, 99:III, 127.

Mathewson, D.S., Broten, N.W. and Cole, D.J., 1965, Aust. J. Phys., 18, 665-667.

Mattingly, R.D., Angulo, E.D., Calabrese, M.A., Tyler, A.L., Tumulty, W.T., Sours, W.P., and Burdick, H.F., 1970, Mechanical Design of Radio Astronomy Explorer (4), NASA Document X-723-70-255.

Mills, B.Y., 1964, Annual Reviews of Astron. and Astrophys., 2, 185.

Novaco, J.C. and Vandenberg, N.R., 1972, NASA X Document X-693-72-8.

Prentice, A.J.R. and ter Haar, D., 1969, Mon. Not. R. Astr. Soc., 146, 423-444.

Purton, C.R., 1972, Private communication.

Reber, G., 1968, Journal of the Franklin Institute, 285, 1-12.

Reynolds, R.J., Roesler, F.L., and Scherb, F., 1972, Low Intensity Balmer Emissions from the Interstellar Medium and Geocorona, NASA Document X-672-72-259.

Sharpless, Stewart, 1959, Ap. J. Suppl., 4, 257.

Somerlock, C.R. and Krustins, J., 1968, "A Precision Spacecraft Radiometer for Hectometer Wavelengths", NASA Tech Note TND-4634.

Stewart, D. and Redwine, K., 1970," RAE-A data Processing System," NASA Contract NAS 5-11723.

Walsh, D., Haddock, F.T., and Schulte, H.F. 1964, Space Research IV, P. Muller, ed., North-Holland (Amsterdam) p. 935.

Weber, R.R., Alexander, J.K., and Stone, R.G., 1971, Radio Science, 6, 1085.